Chemistry & Biodiversity

WILEY-VCH

CHEMISTRY & BIODIVERSITY

RESEARCH ARTICLE

Azaphenothiazine Conjugates: A New Class of Antimicrobial Compounds

Khushbu Kushwaha[1] | Devan Buchanan[2] | Angel Nkosi[2] | Jatin Jangra[3] | Rajnish Kumar[3] | Sandeep Kumar Singh[4] | Subhash C. Jain[1] | Siva S. Panda[2,5]

[1]Department of Chemistry, University of Delhi, Delhi, India | [2]Department of Chemistry and Biochemistry, Augusta University, Augusta, Georgia, USA | [3]Department of Pharmaceutical Engineering & Technology, Indian Institute of Technology, Banaras Hindu University, Varanasi, Uttar Pradesh, India | [4]Jindal Global Business School, O.P. Jindal Global University, Sonipat, Haryana, India | [5]Department of Biochemistry and Molecular Biology, Augusta University, Augusta, Georgia, USA

Correspondence: Siva S. Panda (sipanda@augusta.edu; sspanda12@gmail.com)

Received: 16 December 2024 | **Revised:** 23 January 2025 | **Accepted:** 18 February 2025

Funding: The work was also supported by the Augusta University Provost's office and the Translational Research Program of the Department of Medicine, Medical College of Georgia at Augusta University.

Keywords: antibacterial | antifungal | azaphenothiazine | pharmacokinetic studies | synthesis

ABSTRACT

Although phenothiazines have been widely explored in medicinal chemistry for over a century, little attention has been paid to their pyridine analogs, azaphenothiazines. This article reports the first synthesis, characterization, and antimicrobial evaluation of *S*-oxide analogs of *N*-aminoalkylated azaphenothiazines as antibacterials and antifungals. The optimized synthetic protocol enabled the production of the desired azaphenothiazine sulfoxides **12a–e** and sulfonyls **14a–e**, respectively. In addition to the x-ray crystal structure of azaphenothiazine sulfoxide intermediate **10**, each target compound was characterized using spectroscopy techniques. All of these were investigated in vitro for antibacterial and antifungal activity against several strains of bacteria and fungi. Biological assays revealed selective antibacterial activity, with sulfoxides (**12a–e**) exhibiting broad inhibition and sulfones (**14a–e**) showing selectivity toward gram-negative bacteria. Compound **12c** demonstrated fourfold higher potency against E*scherichia* coli than the reference drug. In antifungal studies, compound **14c** showed the highest activity (MIC 1.2 μg/mL against C*andida* albicans). Our in silico evaluations utilized molecular dynamic (MD) and docking studies for active-site binding simulations, revealing favorable drug-like properties and pharmacokinetics. Finally, toxicology assays determined all synthesized analogs to be non-toxic to kidney and hepatic tissues. This report highlights the newly described *S*-oxide azaphenothiazine conjugates and their potential as potent antimicrobial agents.

1 | Introduction

Infectious diseases remain a major global health challenge, ranking as the third leading cause of death in developed countries and the second worldwide [1, 2]. Despite the development and commercialization of numerous anti-infective drugs, the rapid emergence of drug resistance in bacteria and fungi poses a significant threat to public health [3–5]. Pathogens have evolved various mechanisms to evade the effects of antimicrobial agents, such as producing enzymes that degrade drugs, modifying drug targets to render them ineffective, and expressing efflux proteins that expel the drugs from their cells, reducing their intracellular concentration [6–9]. This escalating resistance has highlighted the urgent need for innovative therapeutic strategies operating through novel mechanisms, minimizing cross-resistance potential. The growing prevalence of infections

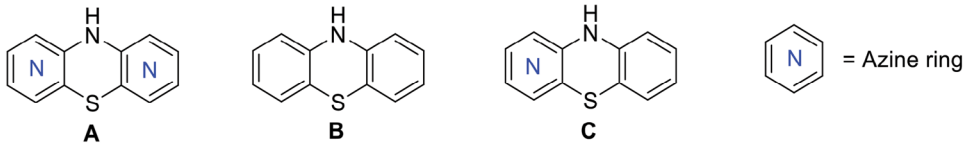

FIGURE 1 | Structure of phenothiazines and azaphenothiazines. (A) Diazaphenothiazine, (B) phenothiazine, and (C) (mono)azaphenothiazine.

driven by antibiotic-resistant bacteria is a pressing health crisis. Misuse and overuse of antibiotics have exacerbated this issue, accelerating the development of resistant strains. As multidrug-resistant pathogens become more common, there is an increasing demand for new antimicrobial agents to combat these resilient organisms effectively [10, 11]. Among the promising candidates are heterocycle-based molecules, which have shown versatile bioactivity, including antimicrobial, antiviral, and anticancer properties. These molecules hold potential as highly specific and non-toxic pharmaceuticals, offering new avenues for drug design [12–16].

Since 1968, there has been a notable absence of new antibiotic classes effective against gram-negative bacteria. Creating new drug-like molecules is essential for understanding bacterial membrane biology and tackling major infectious disease challenges. The aim is to develop therapeutic agents that effectively target and eliminate harmful bacteria and fungi that threaten global public health.

Phenothiazine structures are well-studied heterocyclic scaffolds in medicinal chemistry [17, 18]. They feature a tricyclic ring system containing two benzene rings connected by an amine and sulfide bridge (**B**, Figure 1). Several 10-substituted aminoalkyl phenothiazines were first established as antihistamines [17, 18], antiemetics [19, 20], spasmolytic agents [21], and later, neuroleptics and central nervous system depressants [22]. Structurally related azaphenothiazines (**A** and **C**, Figure 1) are another medicinally relevant class of compounds, differing only by the replacement of one (or both) benzene ring(s) with an azine-type heterocyclic ring(s), such as pyridine, pyridazine, pyrimidine, pyrazine, 1,2,4-triazine, quinoline, quinoxaline, benzoxazine, or benzothiazine. The heteroaromatic systems can contain up to 4 nitrogen atoms, allowing access to more than 50 types of azaphenothiazines, depending on the nature of the fused ring system and the location(s) of the nitrogen atom(s). The variety of possible substructures gives rise to promising biological activities, such as anticancer, antiparasitic, antimicrobial, antipsychotic, and anti-inflammatory (among others) [23–29].

Our group reported the synthesis of novel *bis*-azaphenothiazines containing different alkyl linkers and uncovered interesting antimicrobial activities [30]. Additionally, Morak-Młodawska et al. reported the synthesis of 10-substituted 1,6-diazaphenothiazines and found that the parent compound 1,6-diazaphenothiazine, as well as 10-*N*-substituted propargyl and nitropyridinyl groups were most active against several cancer cell lines [31]. The same group reported the synthesis of previously unknown 10*H*-3,6-diazaphenothiazine and their 10-substituted derivatives. The anticancer studies showed the parent compound 10*H*-3,6-diazaphenothiazine and two diazaphenothiazines, with 2-pyrimidinyl and dimethylaminopropyl substituents at position 10, were selectively active against MCF-7 and C-32 cancer cell lines [32]. Apart from diazaphenothiazines, this group has also reported the synthesis of linearly fused azaphenothiazines—tetracyclic quino[3,2-b]benzo[1,4]thiazines with substituents (H, CH_3, Cl, Br, F, CF_3, SCH_3) in positions 8–10 and aminoalkyl substituents in position 6 and explored their immunological properties. The most active compounds possessed the acetylaminobutyl, chlororoethylureidopropyl, and chloroethylureidobutyl groups and exhibited anticancer activities comparable to cisplatin [33].

Among the possible heteroatom and aromatic substitutions within the azaphenothiazine scaffold, sulfur can assume two higher oxidation states: sulfoxide (*S*-monoxide) and sulfone (S-dioxide). Sulfoxides are highly polar functional groups with strong hydrogen bond-accepting capabilities. Sulfonyls, due to canceling dipoles, are less polar but are categorized as moderate hydrogen bond acceptors [34, 35]. Only a few examples of sulfoxide- and sulfonyl-containing azaphenothiazines and their documented biological activities are cited in the literature. For example, substituted *N*-phenyl 1,3-diazaphenothiazine S-dioxides **I** were tested for antimalarial activity using inhibition of globin proteolysis (IGP) assays, finding derivatives R = H or CH_3 to be most active, having IGP% of 50.09%–92.32% (IGP% positive controls = 24.12%–92.94%). Additionally, 10-*H* and 10-substituted 2,3-diazaphenothiazine-1-one S-dioxides **II** and **III** showed promising analgesic and anti-inflammatory activities similar to their positive control, phenylbutazone [36]. The 10-*H*- and 10-benzyl-substituted 2,3-dichloro-1,4-diazaphenothiazin-5-sulfoxide derivatives **IV** (Figure 2) were evaluated for antimicrobial activity, with compound **IV** (R = H) showed 100% growth inhibition against *Trichophyton mentagrophytes*, *Bacillus subtilis* and *Aspergillus terreus* at a level of 10–100 ppm [37]. Compounds **V** also showed preliminary antimicrobial activity against various bacteria [38]. Derivatives of 1-cyano-3-azaphenothiazin-3*H*(2)-one, sulfoxide (**VI**), and sulfonyl (**VII**) exhibited significant binding properties to the benzodiazepine receptor with IC_{50} = 0.31–0.91 μM [39].

These data suggest such azaphenothiazines containing *S*-oxidation patterns could be a highly valuable area to develop new therapeutics. We viewed this as an opportunity to design and develop potential antibacterial and antifungal agents featuring both *S*-oxidation patterns of azaphenothiazines. The target compounds share a common azaphenothiazine core, characterized by an *N*-substituted lipophilic alkyl bridge linked to one of five possible terminal secondary amines and a sulfoxide or sulfone at the sulfur bridge. Our current effort focused on optimizing synthetic pathways to develop new, diverse *N*-substituted sulfoxide and sulfone azaphenothiazines. Our primary objective was to identify antimicrobial structure–activity relationships (SARs) among all analogs and derive simulated evidence from our findings using in silico techniques. All synthesized conjugates were thoroughly characterized using various spectroscopic techniques.

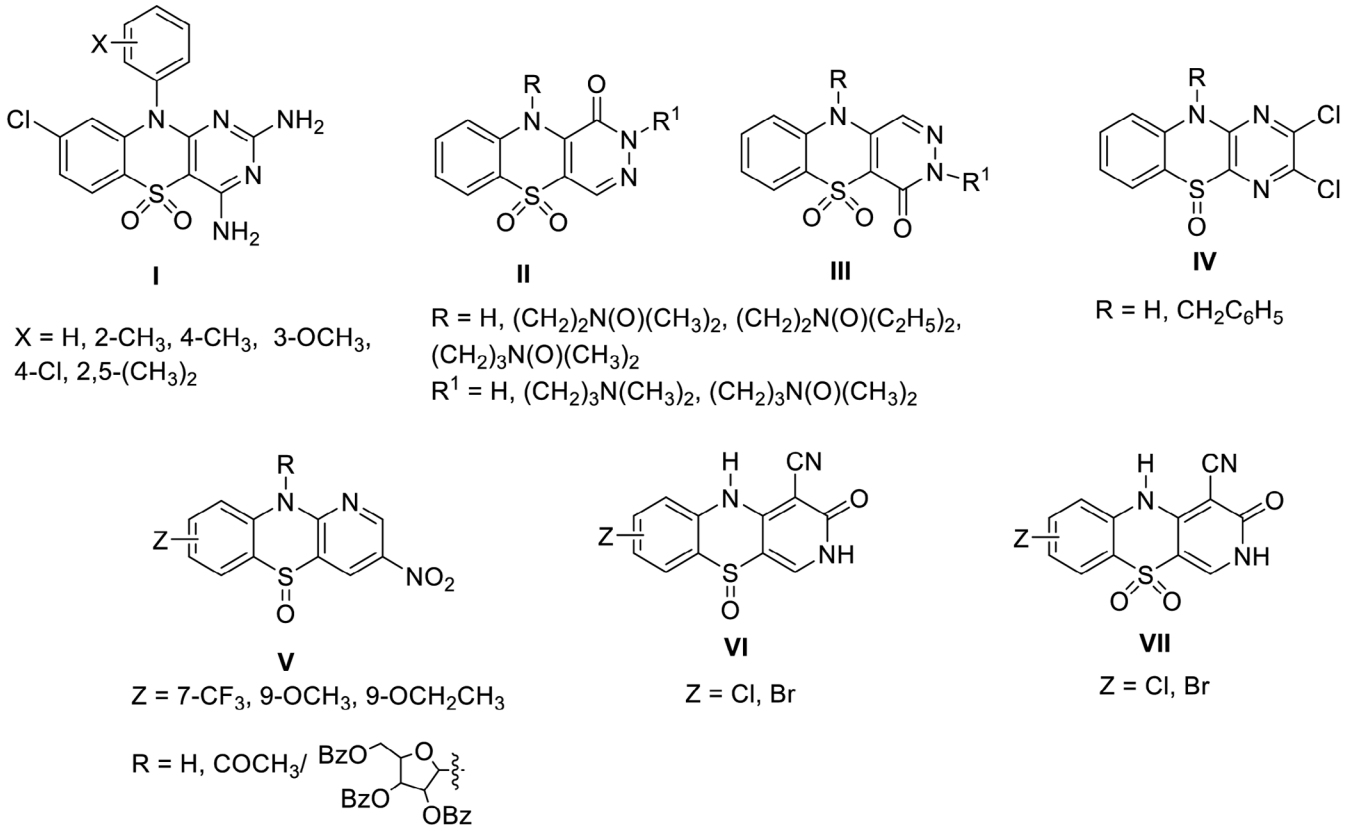

FIGURE 2 | Reported literature examples of sulfoxide and sulfonyl derivatives of aza- or diaza-phenothiazines.

2 | Results and Discussion

2.1 | Chemistry

In Scheme 1, initial efforts to synthesize *N*-alkylated azaphenothiazine **3** followed our reported method [40], treating azaphenothiazine **1** with 1,6-dibromohexane **2** under basic conditions in DMF [41]. However, the yield of desired mono-*N*-alkylated azaphenothiazine **3** was poor after column chromatography.

To address this issue, we pursued an enhanced protocol as outlined in Schemes 2 and 3 that utilized a 3,4-dihydro-2*H*-pyran (DHP) alcohol protecting group. In this alternative approach, 1,6-hexanediol **5** was subject to bromination using HBr in hexanes, utilizing a liquid–liquid extraction. This resulted, primarily, in the production of 6-bromo-1-hexanol **6** as the major product. The –OH group of **6** was protected with DHP using concentrated HCl, leading to the formation of the key intermediate **7** (Scheme 2). DHP-protected **7** was conveniently coupled to azaphenothiazine **1** in the presence of sodium hydride (NaH), producing intermediate **8**, which was subsequently deprotected using *p*-toluene sulfonic acid (*p*-TsOH) in methanol. Finally, intermediate **9** was subject to bromination, using the same liquid–liquid extraction protocol as before, to give the desired mono-*N*-alkylated intermediate **3** in quantitative yield (Scheme 3).

The final compounds under investigation (**12a–e** and **14a–e**) were synthesized using the method outlined in Scheme 4, giving either *S*-sulfoxide- or *S*-sulfonyl-azaphenothiazine tethered to one of five secondary amines. By treatment of 10-(6-bromohexyl)azaphenothiazine **3** under mild oxidizing conditions using *m*-chloroperbenzoic acid (*m*-CPBA), oxidized products **10** and **13** could be obtained up to 91% yield under optimized conditions. The chemoselectivity was therefore affected by controlling the oxidizing agent's molar equivalents. Thus, one molar equivalent of *m*-CPBA (optimized = 1.2 equiv.) resulted in **10** as the major product, while excess (2.5 equiv.) *m*-CPBA led to the production of sulfone **13**. The structural integrity was confirmed using spectroscopic methods (see Supporting Information section) and single-crystal x-ray diffraction (SC-XRD). In the final step, intermediates **10** and **13** were reacted with five secondary amines **11a–e** (piperidine, morpholine, thiomorpholine, *N*-methylpiperazine, or pyrrolidine, respectively) under microwave irradiation (60°C) in the presence of K_2CO_3. This led to a library of five new sulfoxide-containing azaphenothiazines (**12a–e**) and five new sulfonyl-containing azaphenothiazines (**14a–e**). Microwave irradiation was found to be superior to conventional methods regarding purity and yield.

2.2 | X-Ray Studies

The x-ray crystallographic data for the key intermediate **10** (molecular formula: $C_{17}H_{19}BrN_2OS$) was analyzed using the checkCIF/PLATON report, which reveals important structural and refinement details. The orthorhombic unit cell has dimensions a = 15.6079(8) Å, b = 22.4847(9) Å, c = 4.6998(2) Å, and a volume of 1649.34(13) Å^3, with space group Pna21. The molecular weight (MW) is 379.31 g/mol, and the density is 1.528 g/cm^3, measured at 293 K. The refinement yielded an R1 value of 0.0376

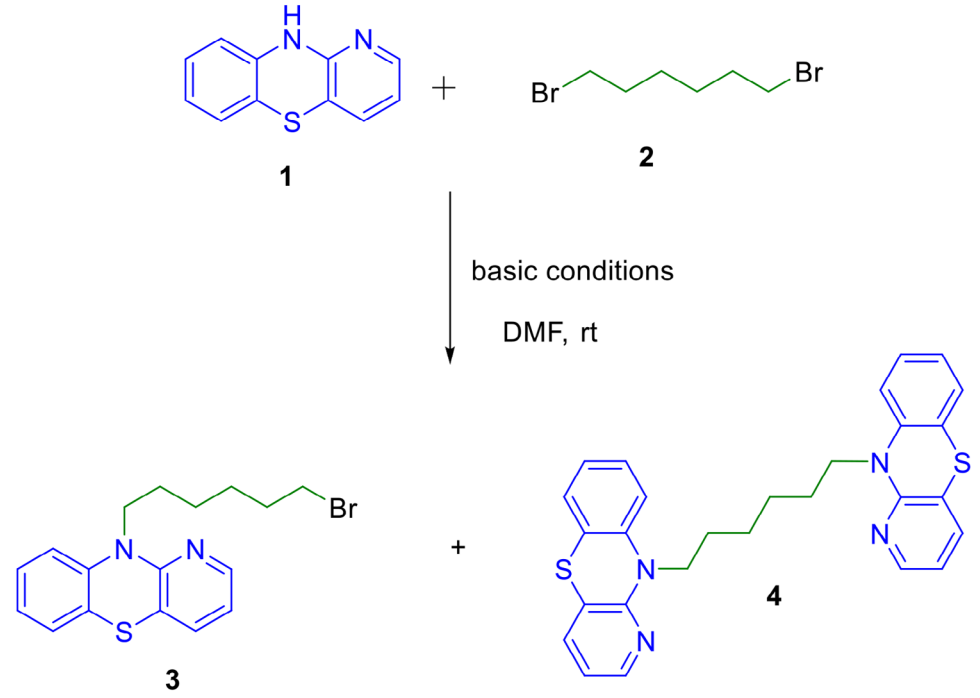

SCHEME 1 | Traditional synthetic protocol for the synthesis of compound **3**.

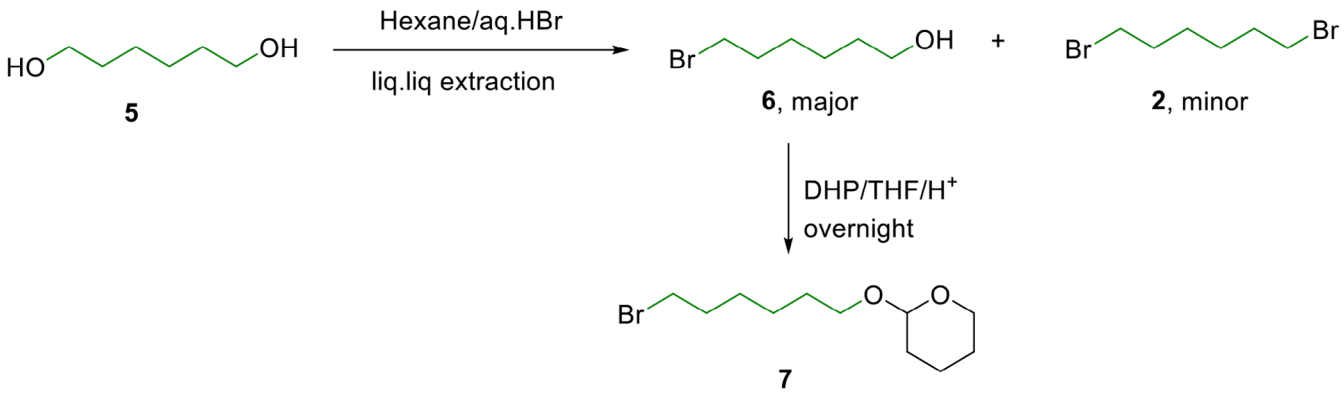

SCHEME 2 | Synthesis of compound **7**.

and a wR2 of 0.0648, with a goodness of fit (S) of 0.822, indicating a good model fit. Data completeness was 126.49%, with 3066 reflections measured to a maximum theta of 28.87°. However, there are several significant alerts. A Level B alert points to a Hirshfeld test deviation between atoms C2 and C3, suggesting potential local disorder or overestimated thermal motion. Level C alerts highlight a short H…H contact at 1.95 Å and a discrepancy in the reported and calculated H_{max} values. Additionally, general alerts suggest inconsistencies in the reported hkl values and a slight deviation of the Flack parameter from zero, which may indicate non-centrosymmetry. Although the structure is well-refined, addressing these alerts, especially those related to the Hirshfeld test and close H…H contact, is necessary to ensure the structure's accuracy and clarity (Figure 3).

Deposition number https://www.ccdc.cam.ac.uk/services/structures?id=https://doi.org/10.1002/cbdv.202403338⟩2418834 (for 10) contain(s) the supplementary crystallographic data for this article. These data are provided free of charge by the joint Cambridge Crystallographic Data Centre and Fachinformationszentrum Karlsruhe http://www.ccdc.cam.ac.uk/structures⟩Access Structures service.

2.3 | Biology Evaluation and SAR

2.3.1 | Antibacterial Studies

The antibacterial properties of the synthesized azaphenothiazine conjugates **12a–e** and **14a–e** were thoroughly investigated. The study employed a range of gram-positive bacteria (*Staphylococcus aureus* ATCC#25923, *B. subtilis* ATCC#6051, and *Staphylococcus epidermidis* ATCC#12228) and gram-negative bacteria (*Escherichia coli* ATCC#25922, *Salmonella typhi* ATCC#19430, *Pseudomonas aeruginosa* ATCC#27853, and *Klebsiella pneumoniae* ATCC#13883). The standard agar dilution technique [42–44] was meticulously utilized to ensure the reliability of the results.

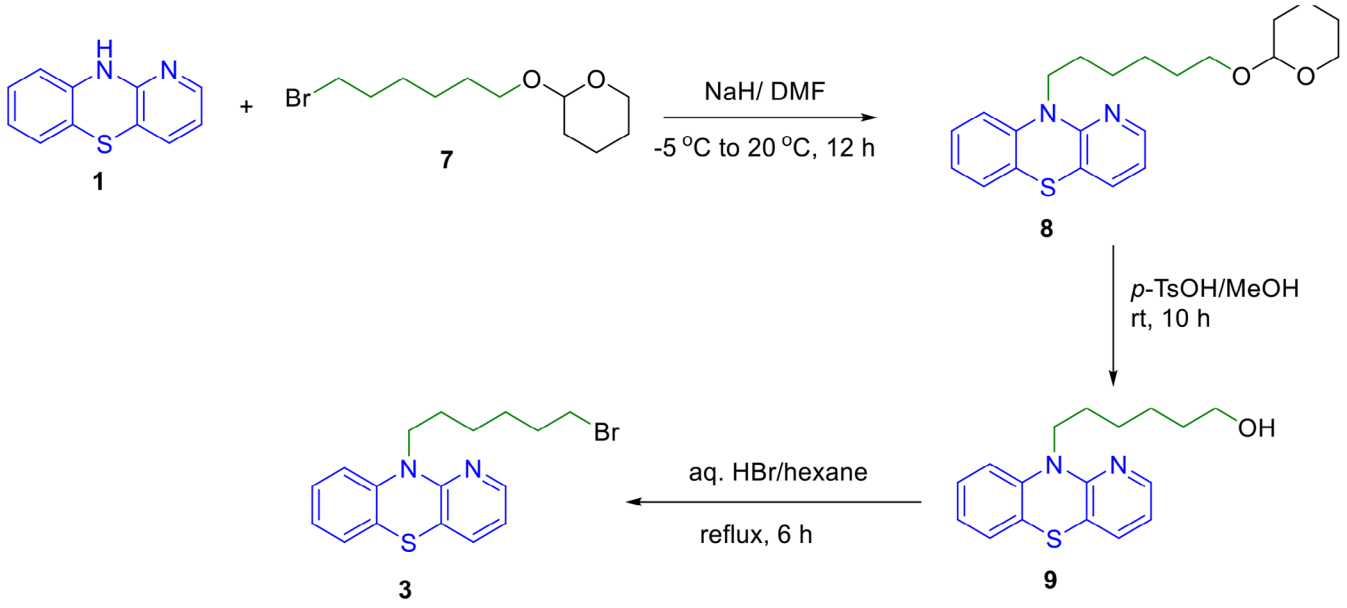

SCHEME 3 | Improved synthetic protocol for compound **3**.

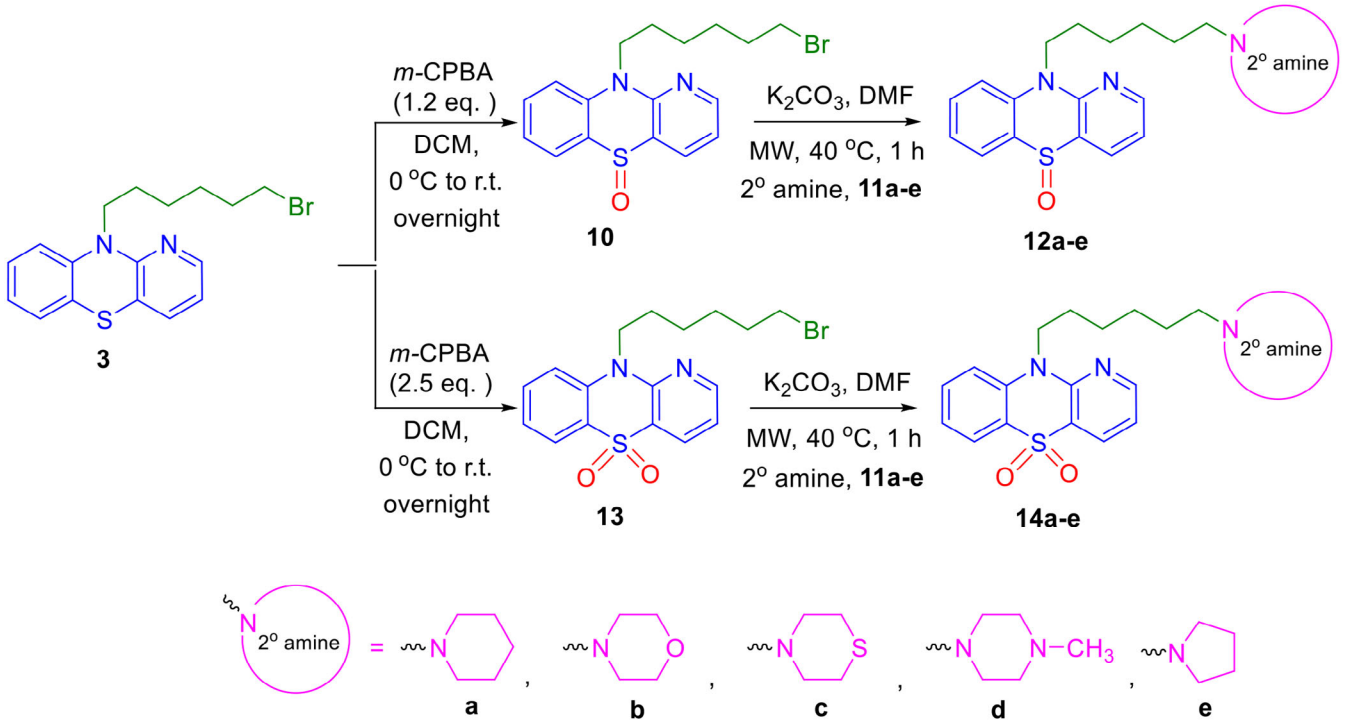

SCHEME 4 | Synthesis of compounds **12a–e** and **14a–e**.

Our study assessed the effectiveness of different compounds in fighting various bacterial strains by measuring their minimum inhibitory concentrations (MICs) outlined in Table 1. Ciprofloxacin, a well-known antibiotic, consistently showed the lowest MIC values across most bacterial strains, indicating its superior effectiveness to compounds **12a–e** and **14a–e**. The MICs of the tested compounds varied significantly, demonstrating varying effectiveness against different bacteria. For example, compound **12b** exhibited low MICs for *S. typhi* and *P. aeruginosa*, but high MICs for *K. pneumoniae*, suggesting a broad but inconsistent effectiveness. Specifically, compound **12d** exhibited a MIC of 1.2 μg/mL against *S. aureus*, whereas compound **14a** showed an MIC of 1.2 μg/mL against *B. subtilis*. Compounds **12b** and **12d** demonstrated a 2.4 μg/mL MIC against *S. epidermidis*. Furthermore, compound **12c** revealed an MIC of 0.6 μg/mL against *E. coli*, and compound **12b** displayed an MIC of 1.2 μg/mL against *S. typhi*. Moreover, compounds **12b** and **12d** exhibited a 1.2 μg/mL MIC against *P. aeruginosa*. However, none of the synthesized conjugates showed effectiveness against *K.* pneumoniae. This variability emphasizes the need to customize

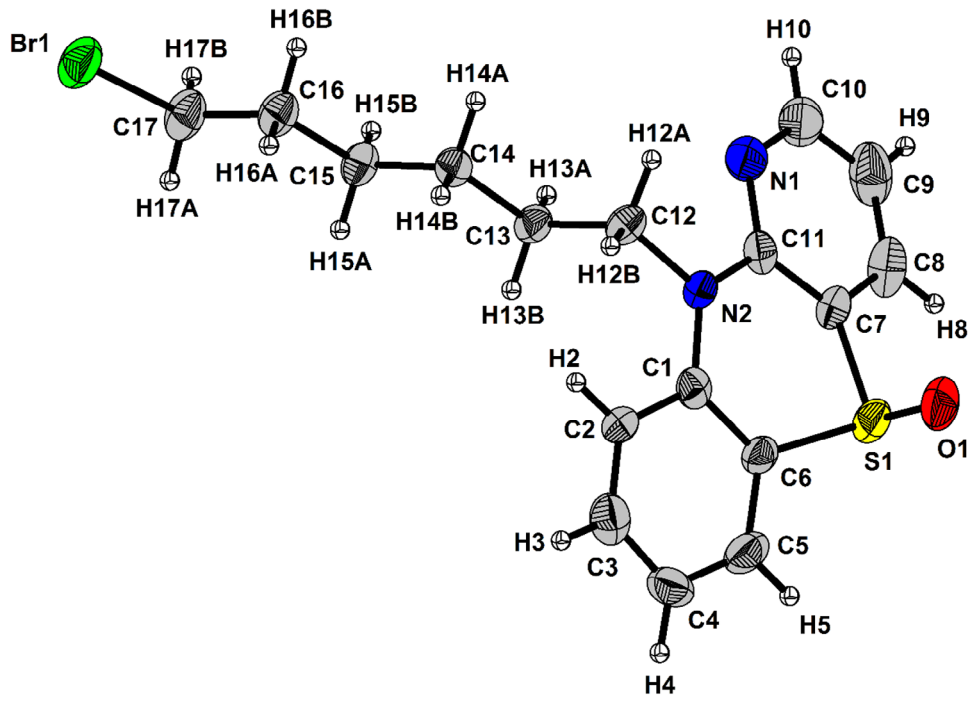

FIGURE 3 | ORTEP diagram of the title compound **10**.

TABLE 1 | Antibacterial activities of the synthesized azaphenothiazine conjugates **12a–e** and **14a–e**.

Compound	Minimum inhibitory concentrations (MIC) (μg/mL)						
	Staphylococcus aureus	***Bacillus subtilis***	***Staphylococcus epidermidis***	***Escherichia coli***	***Salmonella typhi***	***Pseudomonas aeruginosa***	***Klebsiella pneumoniae***
12a	2.4	4.8	4.8	4.8	16	32	4.8
12b	4.8	4.8	2.4	2.4	1.2	1.2	32
12c	4.8	2.4	4.8	0.6	4.8	2.4	4.8
12d	1.2	4.8	2.4	2.4	2.4	1.2	16
12e	16	4.8	8	4.8	16	8	16
14a	4.8	1.2	4.8	2.4	16	4.8	2.4
14b	2.4	4.8	4.8	2.4	4.8	2.4	4.8
14c	2.4	4.8	4.8	4.8	4.8	16	2.4
14d	4.8	16	4.8	4.8	2.4	4.8	16
14e	4.8	4.6	8	8	16	16	8
Ciprofloxacin	0.4	2.8	3.4	2.4	2.4	3.1	1.5

antimicrobial treatments based on the specific bacterial strain and the compound's activity. Our findings underscore the importance of regularly evaluating and comparing antimicrobial agents to ensure the best therapeutic outcomes and effectively address emerging bacterial resistance patterns. Additionally, compound **12c** demonstrated selective effectiveness against *E. coli* with an MIC value of 0.6 μg/mL, which is four times more potent than ciprofloxacin.

The observed data indicate that most synthesized conjugates show selective antimicrobial properties instead of a broad spectrum. Broad-spectrum antibiotics have saved countless lives till now. However, excess use of broad-spectrum antibiotics causes multiple bacteria to acquire resistance. Resistance to broad-spectrum antibiotics is detrimental irrespective of pathogens or commensals. Resistant commensals could act as a reservoir of resistant genes. Furthermore, a broad-spectrum antibiotic eradicates pathogens and beneficial microbes simultaneously. Therefore, selective spectrum antibiotics and current interest could be applied as subtractive therapies. Our results are interesting, and investigating and exploring our scaffold for developing potential antimicrobial agents will be worthwhile.

2.4 | Antifungal Studies

The antifungal properties of the synthesized azaphenothiazine conjugates **12a–e** and **14a–e** were thoroughly investigated in this

TABLE 2 | Antifungal activities of the synthesized azaphenothiazine conjugates **12a–e** and **14a–e**.

Compound	Minimum inhibitory concentrations (MIC) (μg/mL)			
	Aspergillus niger	***Aspergillus fumigatus***	***Aspergillus flavus***	***Candida albicans***
12a	64	16	64	32
12b	64	32	8	64
12c	64	16	64	16
12d	128	16	32	64
12e	64	16	8	64
14a	64	64	64	64
14b	64	64	32	64
14c	64	32	32	1.2
14d	64	32	8	64
14e	64	64	16	64
Amphotericin B	0.31	0.48	0.24	0.39

study. A variety of fungal strains, including *Aspergillus niger* ATCC#16888, *Aspergillus fumigatus* ATCC#96918, *Aspergillus flavus* ATCC#16883, and *Candida albicans* ATCC#18804, were employed. The study rigorously utilized the standard agar dilution technique [37–39] to ensure the reliability of the results.

In this study, we assessed the antifungal activity of various compounds against four fungal species, using Minimum Inhibitory Concentrations (MICs). Amphotericin B, a well-known antifungal agent, demonstrated exceptional potency with low MICs, highlighting its superior efficacy to the tested compounds (Table 2). In contrast, the MIC values for compounds **12a** through **14d** exhibited a broader range, reflecting variable antifungal activity. Compound **12c** showed notable efficacy against *A. fumigatus* and *C. albicans* with MICs of 16 μg/mL, and compound **14c** was particularly effective against *C. albicans* with a remarkably low MIC of 1.2 μg/mL. However, other compounds, such as **12d** and **14a**, exhibited high MICs across multiple species, indicating lower antifungal activity. This variability underscores the need to carefully select antifungal agents based on their specific activity profiles against different fungal pathogens. The comparative analysis reinforces the utility of Amphotericin B as a highly effective treatment option. The observed data emphasize the importance of continually developing and evaluating new antifungal compounds to tackle the varying susceptibility patterns that have been observed. The data on antifungal agents underscore the need for more SAR studies and the synthesis of sulfonyl azaphenothiazine derivatives, which could lead to discovering new and effective antifungal agents.

2.5 | In Silico Studies

2.5.1 | Molecular Docking Study

Molecular docking studies were performed to evaluate the binding interactions of the synthesized compounds along with the reference standard ciprofloxacin against the active site of the *E. coli* DNA gyrase enzyme (PDB ID: 7P2M). The docking results displayed in Table 3 revealed significant binding affinities for the ligands, with compound **12c** exhibiting a docking score of −8.35 kcal/mol, whereas ciprofloxacin showed a slightly lower score of −7.96 kcal/mol, indicating comparable yet distinct binding profiles.

The synthesized compound **12c** demonstrated multiple interactions with the active-site residues of the enzyme (Figure 4A,B). Key hydrogen bonds were formed between the carbonyl oxygen of **12c** and GLY77, ARG136, and VAL167, stabilizing the ligand within the binding pocket. The phenyl and hydrophobic side chains of **12c** contributed to C—H bonds with ASP73 and π–alkyl interactions with VAL43, ALA47, and ILE78. The π–anion interactions observed with the carboxylic acid group of Glu50 and the positively charged guanidine group of ARG76 further reinforced the ligand's electrostatic interactions. Notably, a sulfur-X interaction involving VAL71 highlighted a unique feature of compound **12c**, indicating its potential to exploit underutilized binding site properties. These interactions collectively highlight the ligand's dual ability to engage both hydrophilic and hydrophobic regions of the enzyme's active site.

Ciprofloxacin, the reference compound, also exhibited robust interactions with the active-site residues of the enzyme, albeit with a slightly lower docking score (Figure 4C,D). Key hydrogen bonds were observed between the carbonyl and hydroxyl groups of ciprofloxacin and residues SER112 and THR165, respectively, anchoring the molecule firmly in the binding pocket. The bicyclic quinolone core of ciprofloxacin interacted through π–alkyl contacts with ALA47, VAL71, ILE78, VAL120, and VAL167, emphasizing its hydrophobic engagement. Additionally, an amide–π stacked interaction with ASN46 provided further stabilization, reflecting ciprofloxacin's well-established binding mode against DNA gyrase. Ciprofloxacin interactions spanned polar and hydrophobic regions of the binding pocket, underscoring its balanced binding profile.

Comparatively, compound **12c** showed a slightly stronger binding affinity, as evidenced by its better docking score and unique

TABLE 3 | Docking scores of the synthesized compounds (**12a–e** and **14a–e**) and their corresponding amino acid interactions with the *Escherichia coli* DNA gyrase enzyme.

Compound	Docking score (kcal/mol)	Amino acid interactions between *E. coli* DNA gyrase and the ligand
12a	−9.48	Hydrogen bond (GLY77, ARG136), π–anion (GLU50, ARG76), π–alkyl (VAL43, ALA47, VAL71, ILE78, PRO79, ILE94, VAL120, VAL167)
12b	−9.21	Hydrogen bond (GLY77), C—H bond (VAL43, ASP73), π–anion (GLU50), π–alkyl (ILE78, PRO79, VAL120, VAL167), π–sigma (ILE94)
12c	−8.35	Hydrogen bond (GLY77, ARG136, VAL167), C—H bond (ASP73), π–anion (GLU50, ARG76), π–alkyl (VAL43, ALA47, ILE78), sulfur-X (VAL71)
12d	−9.45	C—H bond (VAL71, ASP73, THR165), π–anion (GLU50), π–alkyl (ILE78, PRO79, ILE94, VAL120, VAL167), amide–π stacked (GLY77)
12e	−7.88	Hydrogen bond (ARG76, GLY77), C—H bond (SER112, THR165), π–anion (GLU50), π–alkyl (ALA53, ILE78, ILE94), π–sigma (PRO79), amide–π stacked (ASN46)
14a	−8.76	Hydrogen bond (GLU50, ARG76, GLY77), C—H bond (ASP73, ILE78, PRO79), π–alkyl (VAL43, ALA47, VAL71, VAL120, VAL167), π–sigma (ILE94)
14b	−9.01	Hydrogen bond (MET95), C—H bond (ILE78), π–alkyl (VAL43, ALA47, VAL71, VAL120, VAL167), π–sigma (THR165), π–sulfur (MET95)
14c	−8.72	Hydrogen bond (MET95), π–alkyl (VAL43, ALA47, VAL71, ARG76, VAL120, VAL167), π–sigma (ILE78, THR165), amide–π stacked (ASN46)
14d	−9.18	C—H bond (VAL43, GLU50, ASP73, SER112, THR165), π–alkyl (ALA47, VAL71, VAL120, VAL167), π–sigma (ILE78), amide–π stacked (ASN46)
14e	−9.10	Hydrogen bond (MET95), π–alkyl (VAL43, ALA47, VAL71, ARG76, PRO79, ILE94, VAL120, VAL167), π–sigma (ILE78, THR165), amide–π stacked (ASN46)
Ciprofloxacin (reference)	−7.96	Hydrogen bond (SER112, THR165), C—H bond (VAL43, ASP73), π–alkyl (ALA47, VAL71, ILE78, VAL120, VAL167), amide–π stacked (ASN46)

interactions, such as the sulfur-X interaction with VAL71, which were absent in ciprofloxacin. The results suggest that the synthesized compound **12c** effectively utilizes the diverse physicochemical environment of the active site, potentially offering an advantage in binding efficiency and specificity.

3 | Molecular Dynamics (MD) Simulation Studies

To comprehensively understand the dynamic behavior of the protein–ligand complex and assess the stability and interaction profile of compound **12c** under physiological conditions, a 200 ns MD simulation was performed using the *E. coli* DNA gyrase structure (PDB: 7P2M) with compound **12c** as the lead molecule. Ciprofloxacin, a well-characterized DNA gyrase inhibitor, served as the reference ligand for comparative analysis.

The root-mean-square deviation (RMSD) plot provided insights into the overall stability of the protein–ligand complex during the simulation. Compound **12c** exhibited an RMSD value of 1.680 nm, indicating moderate stability, whereas ciprofloxacin displayed a lower and more stable RMSD value of 0.901 nm (Table 4). The RMSD for compound **12c** showed significant deviation after approximately 150 ns, which could be attributed to the conformational flexibility of the longer alkyl side chain (Figure 5A). This side chain likely underwent rearrangement within the binding pocket but regained stability thereafter. In contrast, ciprofloxacin maintained a stable binding conformation throughout the simulation, underscoring its superior structural rigidity and stability.

The root-mean-square fluctuation (RMSF) analysis elucidated the dynamic flexibility of amino acid residues and the ligand within the protein's binding site. The protein RMSF values for the **12c** and ciprofloxacin complexes were comparable, with minor differences (0.177 and 0.179 nm, respectively). Residues proximal to the binding pocket exhibited notable flexibility, potentially contributing to interaction dynamics. Ligand RMSF analysis revealed greater flexibility for compound **12c** (0.174 nm) compared to ciprofloxacin (0.099 nm), suggesting that the extended alkyl chain of **12c** contributes to dynamic conformational adjustments within the active site, whereas ciprofloxacin's relatively rigid structure resulted in lower fluctuations (Figure 5B,C).

The radius of gyration (Rg) was monitored to evaluate the compactness of the protein structure during the simulation [45]. Compound **12c** and ciprofloxacin demonstrated comparable Rg values of 1.763 and 1.764 nm, respectively (Figure 5D). This consistency suggests that both ligands maintained the structural integrity of the protein, with minimal conformational deviations observed during the simulation. The solvent-accessible surface area (SASA) analysis revealed higher values for the **12c** complex (121.83 nm^2) compared to the ciprofloxacin complex (118.49 nm^2) (Figure 5E). This difference could be attributed to

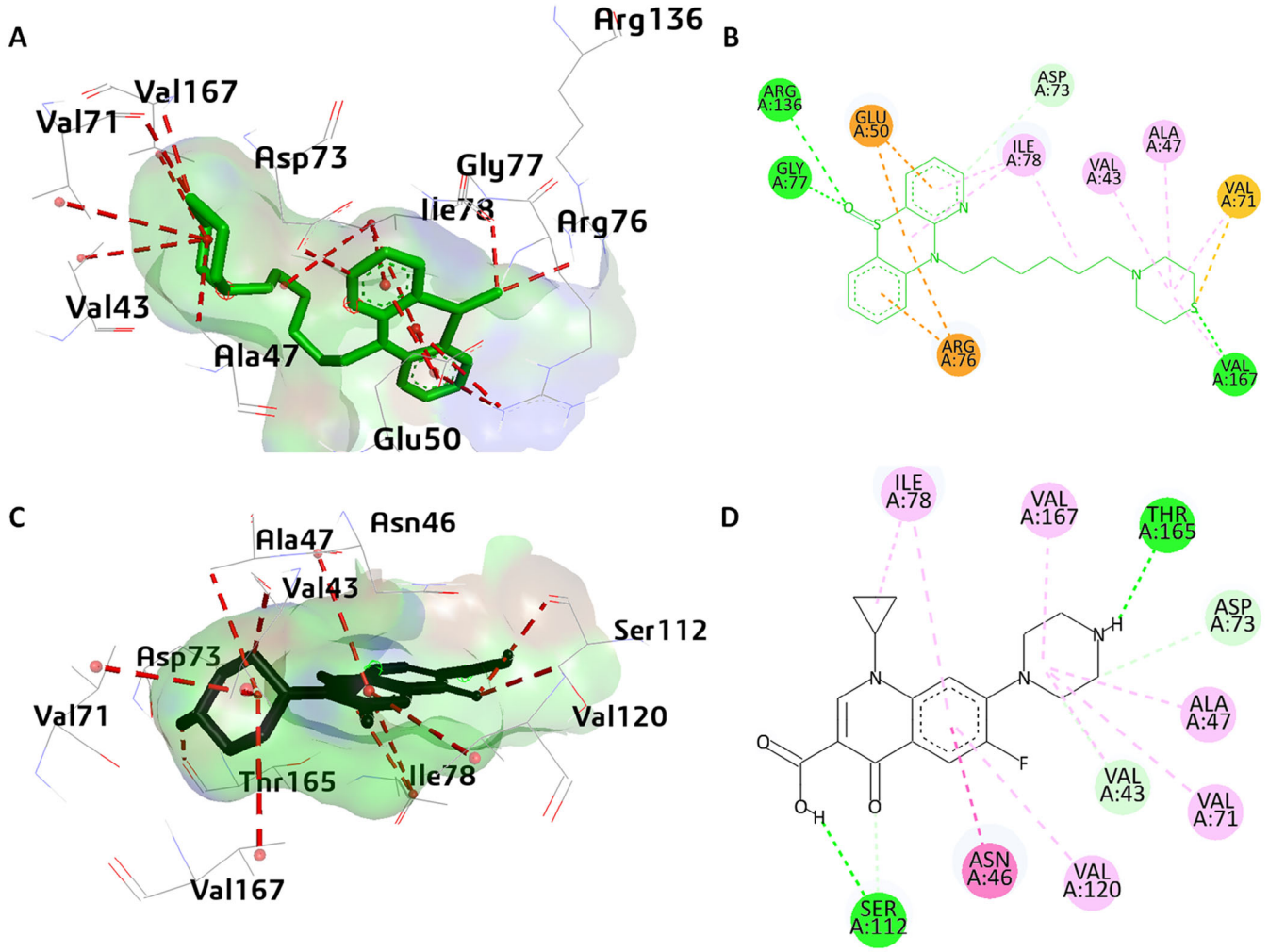

FIGURE 4 | 3D binding pose and 2D representation of docking interactions for the lead compound **12c** (A and B) and ciprofloxacin as reference (C and D).

TABLE 4 | Molecular dynamic (MD) analysis data for the lead compound, **12c**, along with the reference protein–ligand complex (ciprofloxacin).

Parameters	Compounds in complex with *Escherichia coli* DNA gyrase	
	12c	**Ciprofloxacin (reference ligand)**
RMSD (nm)	1.680	0.901
Protein RMSF (nm)	0.177	0.179
Ligand RMSF (nm)	0.174	0.099
Rg (nm)	1.763	1.764
SASA (nm^2)	121.83	118.49

Abbreviations: Rg, radius of gyration; RMSD, root-mean-square deviation; RMSF, root-mean-square fluctuation; SASA, solvent-accessible surface area.

the increased conformational flexibility and the extended alkyl chain of **12c**, which may expose a larger surface area to the solvent [46].

Hydrogen bond formation is critical for ligand binding and stabilization. Compound **12c** established consistent hydrogen bonds with the protein, with the number of bonds fluctuating between two and five throughout the simulation (Figure 5G). This fluctuation indicates dynamic but stable interactions, likely facilitated by the flexible functional groups of **12c**. Ciprofloxacin, in comparison, maintained a similar hydrogen bond range but demonstrated more stability in bond formation due to its rigid structure and well-optimized binding mode. The hydrogen bond distance distribution for both complexes revealed similar peaks, indicating comparable interaction strengths (Figure 5F). The stable hydrogen bonding interactions suggest that compound **12c**

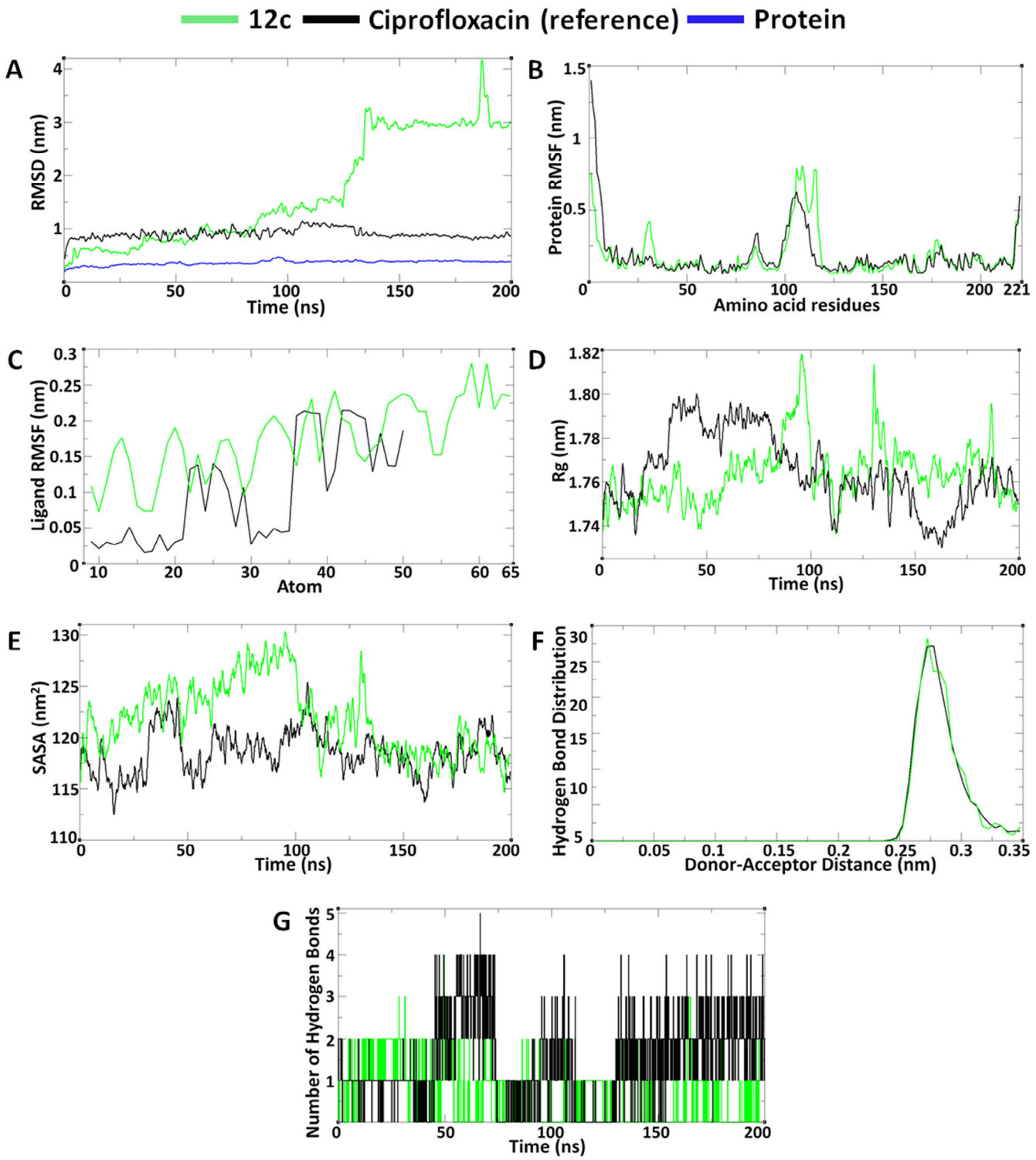

FIGURE 5 | MD simulation data for the lead compound **12c** (green) with comparison to the reference ligand (**ciprofloxacin** in black) in complex with *Escherichia coli* DNA gyrase enzyme (PDB ID: 7P2M): (A) RMSD plot, (B) protein RMSF plot, (C) ligand RMSF plot, (D) radius of gyration (Rg) plot, (E) solvent-accessible surface area (SASA) plot, (F) H-bond distribution (within 0.3 nm distance), and (G) number of intermolecular hydrogen bonds formed between protein–ligand complex throughout the simulation run of 200 ns. RMSD, root-mean-square deviation; RMSF, root-mean-square fluctuation.

is capable of forming robust connections with the protein despite its higher RMSD.

Although ciprofloxacin demonstrated superior stability and compactness as a reference ligand, compound **12c** exhibited notable flexibility and adaptability within the binding pocket. The increased ligand RMSF and SASA values for **12c** suggest a dynamic binding mode, likely influenced by the flexible alkyl side chain (Table 4). This flexibility could be advantageous in scenarios where adaptable interactions are beneficial. However,

TABLE 5 | In silico pharmacokinetic properties of azaphenothiazine conjugates **12a–e** and **14a–e**.

Compound	MW	nHBA	nHBD	nRB	logP	TPSA	MR	HIA	BBB	Lipinski
12a	383.55	3	0	7	4.04	55.65	119.19	High	Yes	Yes
12b	385.52	4	0	7	2.82	64.88	115.47	High	Yes	Yes
12c	401.59	3	0	7	3.62	80.95	121.98	High	No	Yes
12d	398.56	4	0	7	3.00	58.89	126.00	High	Yes	Yes
12e	369.52	3	0	7	3.68	55.65	114.39	High	Yes	Yes
14a	399.55	4	0	7	4.05	61.89	119.88	High	Yes	Yes
14b	401.52	5	0	7	2.83	71.12	116.16	High	Yes	Yes
14c	417.59	4	0	7	3.63	87.19	122.66	High	No	Yes
14d	414.56	5	0	7	3.02	65.13	126.69	High	Yes	Yes
14e	385.52	4	0	7	3.69	61.89	115.07	High	Yes	Yes

Abbreviations: BBB, blood–brain barrier; HIA, human intestinal absorption; MW, molecular weight; nRB, number of rotatable bonds; TPSA, total polar surface area.

the moderate RMSD and stable hydrogen bond interactions highlight the potential of compound **12c** as a lead molecule for further optimization. The structural features of **12c**, particularly its longer alkyl side chain, make it a promising candidate for refinement to enhance binding stability and reduce fluctuations.

3.1 | Absorption, Distribution, Metabolism, and Excretion (ADME) Studies

A computational analysis was conducted to predict the synthesized compounds' pharmacokinetic properties. The study focused on pharmacokinetic parameters such as ADME. These parameters are essential in developing new drugs, as compounds with suboptimal ADME profiles often fail in clinical trials. The properties of the compounds were evaluated using the Lipinski *"Rule of Five"* and drug-likeness and drug-score metrics through STARDROP and SwissADME tools [47, 48].

Lipophilicity, in particular, plays a significant role in a drug's antimicrobial effects as it directly affects the compound's ability to permeate biological membranes. Compounds with high lipophilicity are distributed into hydrophobic compartments, such as cell lipid bilayers, whereas those with lower lipophilicity are more likely to remain in hydrophilic environments like blood serum. Lipophilicity influences the distribution, metabolism, and excretion of drugs within the body. Additionally, many proteins involved in drug transport and metabolism have hydrophobic binding sites, emphasizing the importance of a compound's lipophilic character for its overall pharmacological activity.

The Lipinski "Rule of Five" considers key factors influencing oral bioavailability, including lipophilicity (cLogP ≤ 5), hydrogen bond acceptors (nHBA ≤ 10), hydrogen bond donors (nHBD ≤ 5), and MW ≤ 500 Da. In addition, other drug-like properties, such as total polar surface area (TPSA ≤ 140 Å^2), human intestinal absorption (HIA), molar index, and the number of rotatable bonds (nRB < 10), play essential roles in drug development (Table 5). In addition, the ability to cross the blood–brain barrier (BBB) is another aspect of antimicrobial drugs based on the need. These properties are critical for predicting a compound's oral active potential [49].

The term "chemical universe," often referred to as "chemical space" or "chemical compound space," encompasses the entire set of possible molecules characterized by a multi-dimensional space that captures their functional and structural properties, as well as the interrelationships among them. Although this concept can be applied to any molecule, it has been most extensively studied with small, quantitative, and qualitative organic compounds [50–52]. To assess the drug-like properties of the synthesized conjugates, we analyzed their physicochemical space, representing these molecules in a multi-dimensional space that highlights their functional and structural attributes (Table 6).

3.2 | Toxicity Studies

Antimicrobials are frequently linked to significant toxicities [53–56]. These can include drug-induced liver injury (DILI) [57], nephrotoxicity [58], and neurotoxicity [59]. Common agents such as isoniazid, rifampin, aminoglycosides, and metronidazole often lead to adverse effects through mechanisms like oxidative stress, mitochondrial dysfunction, and immune-mediated damage. In this study, we predicted the toxicity of the synthesized conjugates using ProTox-3.0 [60], and the findings are summarized in Table 7. The predictive data suggest all the synthesized conjugates do not show toxicity for the liver and kidney. However, all the conjugates have the possibility of neurotoxicity except **14b**. Our most potent compound, **12c**, also has the possibility of neurotoxicity, but interestingly, it has no permeability for BBB.

4 | Conclusion

In summary, we have developed an efficient synthetic pathway to produce ten S-oxide azaphenothiazine conjugates in excellent yields. We have thoroughly characterized all products using standard spectroscopic techniques. Furthermore, we have assessed all synthesized conjugate's antibacterial and antifungal properties. Sulfoxide azaphenothiazines **12a–e** exhibited potent

TABLE 6 | Physiochemical space of azaphenothiazine conjugates **12a–e** and **14a–e**.

12a	**12b**	**12c**	**12d**	**12e**
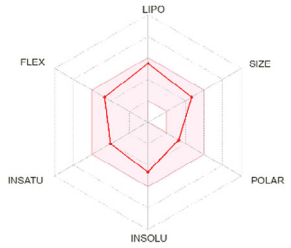	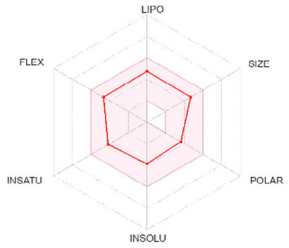	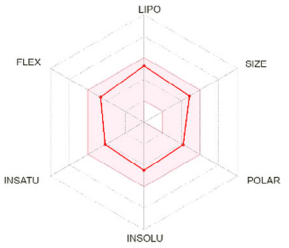	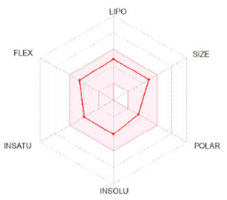	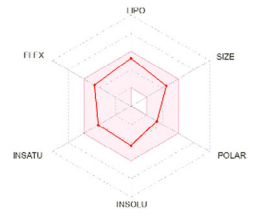
14a	**14b**	**14c**	**14d**	**14e**
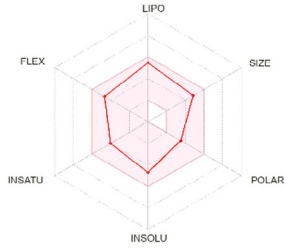	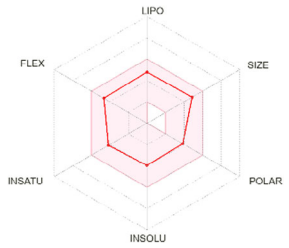	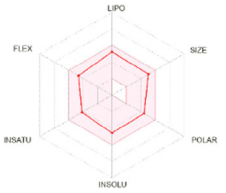	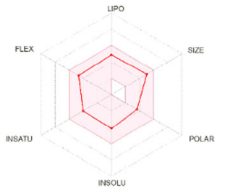	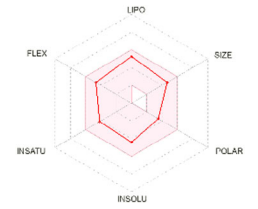

TABLE 7 | Predicted toxicity data.

Compound	Probability			LD_{50} (mg/kg)
	Hepatotoxicity	Neurotoxicity	Nephrotoxicity	
12a	0.74 (−ve)	0.71 (+ve)	0.85 (−ve)	502
12b	0.72 (−ve)	0.62 (+ve)	0.69 (−ve)	502
12c	0.74 (−ve)	0.71 (+ve)	0.85 (−ve)	502
12d	0.70 (−ve)	0.72 (+ve)	0.84 (−ve)	503
12e	0.75 (−ve)	0.72 (+ve)	0.86 (−ve)	502
14a	0.74 (−ve)	0.63 (+ve)	0.76 (−ve)	502
14b	0.69 (−ve)	0.51 (−ve)	0.66 (−ve)	502
14c	0.74 (−ve)	0.63 (+ve)	0.76 (−ve)	502
14d	0.72 (−ve)	0.65 (+ve)	0.76 (−ve)	503
14e	0.76 (−ve)	0.65 (+ve)	0.75 (−ve)	502

antibacterial activity against both gram-positive (five entries, Table 1) and gram-negative strains, with higher selectivity for gram-negative (eight entries, Table 1). The best of which, product **12c**, demonstrated a fourfold greater MIC (0.6 μg/mL) toward *E. coli* cultures than ciprofloxacin (MIC = 2.4 μg/mL). Predictive toxicity data for **12c** showed no potential for toxicity to the liver and kidney and does not have BBB permeability. The sulfonyl azaphenothiazines (**14a–e**) showed higher spectrum selectivity toward gram-negative bacteria. Compounds **14a**, **14b,** and **14d** showed superior or similar antibacterial activity toward certain gram-negative strains compared to ciprofloxacin. Among the compounds tested, only two, **14a** and **14c**, showed favorable activity against *K. pneumoniae*. This study also highlighted the inactivity of *S*-oxide azaphenothiazines toward fungal strains. However, **14c** did show effective antifungal activity against *C. albicans*, providing an avenue for further SAR investigations to produce potent antifungals containing sulfonyl- or sulfoxide-containing azaphenothiazine scaffolds. Additionally, all products adhere to Lipinski's rule of five guidelines and showed no kidney or hepatic toxicities. However, some products did show the potential to be neurotoxic, despite being impermeable to the BBB. Physiochemical space data also suggest the new *S*-oxide azaphenothiazine derivatives possess drug-like properties, making them promising candidates for further investigation as antimicrobial agents.

5 | Experimental Section

All heterocyclic secondary amines were purchased from commercial suppliers (Sigma Aldrich and Merck) and used as such. 1,6-Dibromohexane was also purchased from Sigma Aldrich. Azaphenothiazine was synthesized by a previously reported method from our group [40, 61], and 2-(6-bromohexyloxy)tetrahydro-2*H*-pyran was synthesized by a literature procedure starting from 6-bromo-1-hexanol [62, 63]. Solvents used in the extraction and purification processes were distilled before use. Products were purified by column chromatography using silica gel as an adsorbent. Melting points were determined using a Tropical Lab equipment and were uncorrected. IR (KBr) and (film) spectra were recorded on a PerkinElmer FTIR spectrophotometer; these values are expressed as ν_{max} cm^{-1}H (^{13}C). NMR spectra were recorded at 400 (100.6) MHz on a Jeol spectrometer and a Bruker spectrometer and at 300 (75.5) MHz on a DPX-300 Bruker spectrometer using $CDCl_3$ or DMSO as a solvent, and TMS (tetramethylsilane) was used as a reference for both ^{1}H and ^{13}C NMR spectrum. Coupling constants *J* values were given in hertz, and the chemical shifts are given in ppm. The coupling patterns were expressed as d (doublet), dd (double doublet), t (triplet), q (quartet), p (pentet), td (triplet of doublet), and so on. Elemental analyses were performed on a PerkinElmer series 11 CHNS/O analyzer 2400. Mass spectra were recorded on a MicroMass AutoSpec LCTKC 455, an Agilent 6310 Ion Trap, and a Jeol SX 102 mass spectrometer.

5.1 | 10-(6-((Tetrahydro-2*H*-Pyran-2-yl)oxy) Hexyl)-10*H*-Benzo[b]Pyrido[2,3-e][1,4]Thiazine (8)

To a cooled solution of sodium hydride (100.0 mmol, 2.4 g) in dry DMF (20 mL), a solution of 10*H*-benzo[b]pyrido[2,3-e][1,4]thiazine (**1**) (50.0 mmol, 10.0 g) in dry DMF (30 mL) was added dropwise under inert atomosphere of nitrogen. The contents were stirred at −5°C to 0°C for 30 min, and then a solution of 2-(6-bromohexyloxy)tetrahydro-2*H*-pyran (**1**) (50.0 mmol, 13.2 g) in 30 mL of DMF was added to it dropwise. Stirring was continued at room temperature for another 14 h. Completion of reaction was monitored by TLC, and then the contents were treated with water and extracted with ethyl acetate. The combined extract was dried over anhydrous sodium sulfate. The solvent was removed under reduced pressure, and the crude product obtained was purified by column chromatography. Elutions with *n*-Hex/EtOAC (90:10) yielded 10-(6-(tetrahydro-2*H*-pyran-2-yloxy)hexyl)-10*H*-benzo[b]pyrido[2,3-e][1,4] thiazine (**8**) as light yellow oil. Yield: 11.7 g (61%), R_f = 0.54 in *n*-Hex/EtOAc (90:10). **IR ν_{max}** (film): 3063, 2937, 2858, 1593, 1568, 1445, 1414, 1375, 1253, 1135, 1077, 1033, 779, 746 cm^{-1}. **^{1}H NMR** (δ, $CDCl_3$, 400 MHz): 7.99–7.97 (dd, 1H, *J* = 5.0 and 1.8 Hz), 7.23–7.21 (dd, 1H, *J* = 7.8 and 2.2 Hz), 7.14–7.10 (m, 1H), 7.04–7.02 (dd, 1H, *J* = 7.3 and 0.9 Hz), 6.91–6.87 (m, 1H), 6.84 (d, 1H, *J* = 8.7 Hz), 6.74–6.70 (m, 1H), 4.56 (t, 1H, *J* = 2.7 Hz, O—C**H**—O), 4.06 (t, 2H, *J* = 8.7 Hz, NC**H$_2$**), 3.87–3.83 (m, 2H, C**H$_2$**-OTHP), 3.50–3.46 (m, 1H, C**H**H—O—, pyran),

3.40–3.34 (m, 1H, CH**H**—O—, pyran), 1.85–1.77 (m, 4H), 1.73–1.67 (m, 2H), 1.62–1.58 (m, 4H), 1.53–1.39 (m, 4H). **^{13}C NMR** (δ, $CDCl_3$, 100 MHz): 155.4, 145.4, 143.2, 134.4, 127.8, 127.4, 123.1, 121.7, 118.0, 117.4, 115.8, 99.2, 67.9, 62.7, 45.2, 31.1, 30.1, 27.2, 26.9, 26.4, 25.8, 20.0. **Mass spectral data,** TOF ES+ *m/z*: 385 [$M^+ + 1$]. **Anal. calcd** for $C_{22}H_{28}N_2O_2S$: C, 68.72; H, 7.34; N, 7.29. Found: C, 68.80; H, 7.33; N, 7.30.

5.2 | 6-(10*H*-Benzo[b]Pyrido[2,3-e][1,4]Thiazin-10-yl)Hexan-1-ol (9)

To a solution of 10-(6-(tetrahydro-2*H*-pyran-2-yloxy)hexyl)-10*H*-benzo[b]pyrido[2,3-e][1,4] thiazine (**8**) (26.0 mmol, 10.0 g) in methanol, catalytic amount of *p*-toluene sulfonic acid (2.6 mmol, 0.44 g) was added. Contents were stirred at room temperature for 10 h. The progress of reaction was monitored on TLC. After completion of the reaction, the solvent was removed under reduced pressure, and the residue left was dissolved in ethyl acetate. The organic solution was washed with sodium bicarbonate solution followed by water. The organic layer was dried over anhydrous sodium sulfate and concentrated under reduced pressure to give a brownish oil that was purified by column chromatography using silica gel as an adsorbent to obtain 6-(10*H*-benzo[b]pyrido[2,3-e][1,4]thiazin-10-yl)hexan-1-ol (**9**) as a light green oil. Yield: 6.1 g (78%), $R_f = 0.36$ in DCM/MeOH (98:2). **IR** ν_{max} (film): 3368, 3062, 2931, 2857, 1593, 1444, 1413, 1375, 1251, 1129, 1046, 779, 746 cm^{-1}. **^{1}H NMR** (δ, $CDCl_3$, 400 MHz): 7.98–7.97 (dd, 1H, J = 4.5 and 1.3 Hz), 7.23–7.21 (dd, 1H, J = 7.3 and 1.8 Hz), 7.14–7.10 (m, 1H), 7.04–7.02 (dd, 1H, J = 7.8 and 1.3 Hz), 6.90–6.86 (m, 1H), 6.84 (d, 1H, J = 7.7 Hz), 6.73–6.70 (m, 1H), 4.06 (t, 2H, J = 7.3 Hz, NC**H$_2$**), 3.61 (t, 2H, J = 6.6 Hz, C**H$_2$**OH), 1.80 (p, 2H, J = 6.8 Hz), 1.57 (p, 2H, J = 6.8 Hz), 1.49–1.37 (m, 4H). **^{13}C NMR** (δ, $CDCl_3$, 100 MHz): 155.0, 144.9, 142.8, 134.2, 127.5, 127.0, 122.7, 121.4, 117.6, 117.2, 115.4, 62.7 (**C**H_2OH), 44.7 (N**C**H_2), 32.6, 26.7, 26.4, 25.4. **Mass spectral data,** TOF ES+ *m/z*: 301 [$M^+ + 1$]. **Anal. calcd** for $C_{17}H_{20}N_2OS$: C, 67.97; H, 6.71; N, 9.32. Found: C, 68.12; H, 6.78; N, 9.30.

5.3 | 10-(6-Bromohexyl)-10*H*-Benzo[b]Pyrido[2,3-e][1,4]Thiazine (3)

Aq. hydrobromic acid 48% (83.0 mmol, 6.70 g) was added to a well-stirred solution of 6-(10*H*-benzo[b]pyrido[2,3-e][1,4]thiazin-10-yl) hexane-1-ol (**9**) (16.6 mmol, 5.0 g) in 100 mL of hexane. The reaction mixture was stirred at room temperature for 10 min and refluxed for 6 h. TLC monitored the progress of the reaction. After the reaction was completed, the reaction mixture was concentrated under a vacuum and poured into ice-cold water. After neutralization with sodium bicarbonate, it was extracted using dichloromethane. The combined chloroform extracts were first washed with water, followed by a brine solution, and the organic layer was dried over anhydrous sodium sulfate, filtered, and the solvent was evaporated under a vacuum. The residue left was purified by column chromatography using silica gel as an adsorbent. Elutions with *n*-Hex/EtOAC (95:5) furnished 10-(6-bromohexyl)-10*H*-benzo[b]pyrido[2,3-e][1,4]thiazine (**3**) as a light yellow oil. Yield: 4.1 g (68%), R_f = 0.63 in *n*-Hex/EtOAc (90:10). **IR** ν_{max} (film): 3061, 2932, 2855, 1592, 1568, 1444, 1413, 1252, 1127, 1044, 780, 746 cm^{-1}. **^{1}H NMR** (δ, $CDCl_3$, 400 MHz): 7.98–7.97 (dd, 1H, J = 4.8 and 1.4 Hz), 7.23–7.21 (dd, 1H, J = 7.6 and 1.6 Hz), 7.12 (td, 1H, 7.4 and 1.2 Hz), 7.04–7.02 (dd, 1H, J = 7.6 and 1.6 Hz), 6.89 (td, 1H, 7.2 and 0.8 Hz), 6.83 (d, 1H, J = 6.3 Hz), 6.73–6.70 (m, 1H), 4.06 (t, 2H, J = 5.4 Hz, NC**H$_2$**), 3.38 (t, 2H, J = 6.8 Hz, C**H$_2$**Br), 1.87–1.80 (m, 4H), 1.47–1.45 (m, 4H). **^{13}C NMR** (δ, $CDCl_3$, 100 MHz): 155.1, 145.1, 142.9, 134.2, 127.6, 127.1, 122.8, 121.5, 117.8, 116.2, 114.6, 44.7 (N**C**H_2), 33.9 (**C**H_2Br), 32.7, 27.9, 26.4, 26.2. **Mass spectral data,** TOF ES+ *m/z*: 364 [$M^+ + 2$]. **Anal. calcd** for $C_{17}H_{19}BrN_2S$: C, 56.20; H, 5.27; N, 7.71. Found: C, 56.41; H, 5.30; N, 7.70.

5.4 | 10-(6-Bromohexyl)-10*H*-Benzo[b]Pyrido[2,3-e][1,4]Thiazin-5-Oxide (10)

To a stirred solution of 10-(6-bromohexyl)-10*H*-benzo[b]pyrido[2,3-e][1,4]thiazine (**3**) (2.0 g, 5.52 mmol) in dry dichloromethane (15 mL) was added *m*-CPBA (1.13 g, 6.61 mmol) in dichloromethane (10 mL) at 0°C under nitrogen atmosphere. The reaction mixture was stirred at 0°C for the next 4 h and then at room temperature for 2 h. Progress of the reaction was monitored by TLC. Solvents were removed in vacuo, and the resulting residue was poured into ice-cold water and extracted with chloroform thrice; organic solutions were combined and dried over anhydrous sodium sulfate. The solvent was removed under vacuum. TLC showed two spots, therefore, column chromatography was done to isolate the major product as 10-(6-bromohexyl)-10*H*-benzo[b]pyrido[2,3-e][1,4]thiazin-5-oxide (**10**) as a white solid. Yield 1.89 g (91%), m.p. 70°C–72°C, R_f = 0.67 in chloroform/methanol (90:10).

IR ν_{max} (KBr): 2932, 2862, 1574, 1451, 1413, 1250, 1149, 1044, 1019, 787, 754, 642, 534 cm^{-1}. **^{1}H NMR (δ, DMSO-d_6, 400 MHz)**: 8.70 (d, 1H, J = 3.9 Hz), 8.43 (d, 1H, J = 7.5 Hz), 8.02 (d, 1H, J = 7.2 Hz), 7.76–7.70 (m, 2H), 7.37–7.29 (m, 2H), 4.58 (m, 2H, —NCH_2), 3.60 (t, 2H, J = 6.3 Hz, —CH_2Br), 1.98–1.71 (m, 4H), 1.43–1.32 (m, 4H). **^{13}C NMR (δ, DMSO—d_6, 100 MHz)**: 152.6, 147.0, 140.7, 136.9, 133.3, 130.7, 123.4, 122.3, 118.0, 117.7, 116.7, 45.2 (—NCH_2), 34.9 (—CH_2Br), 32.1, 27.1, 26.0, 25.1. **Mass spectral data, TOF ES+ *m/z* (%)**: 380 ($M^+ + 2$). **Elemental analysis**: C = 53.85%, H = 5.07%, N = 7.37%, S = 8.42%. **Calculated**: C = 53.83%, H = 5.05%, N = 7.39%, S = 8.45%. **Empirical formula**: $C_{17}H_{19}BrN_2OS$

5.5 | 10-(6-Bromohexyl)-10*H*-Benzo[b]Pyrido[2,3-e][1,4]Thiazin-5,5-Dioxide (13)

To a stirred solution of 10-(6-bromohexyl)-10*H*-benzo[b]pyrido[2,3-e][1,4]thiazine (**3**) (2 g, 5.52 mmol) in dry dichloromethane (15 mL) was added *m*-CPBA (2.36 g, 13.7 mmol) in dichloromethane (30 mL) at 0°C under nitrogen atmosphere. The reaction mixture was stirred at this temperature for 1 h and then continued for 10 h at room temperature. The progress of the reaction was monitored by TLC. Solvents were removed in vacuo, and the resulting residue was poured into ice-cold water and extracted with chloroform thrice; organic solutions were combined and dried over anhydrous sodium sulfate. The solvent was removed under a vacuum. TLC showed two spots; therefore, column chromatography was done to isolate the major product as 10-(6-bromohexyl)-10*H*-benzo[b]pyrido[2,3-e][1,4]thiazin-5,5-dioxide (**13**) as a reddish solid. Yield 1.95 g (90%), m.p. 60°C–62°C, R_f = 0.48 in chloroform/methanol (95:5).

IR ν_{max} (KBr): 2933, 2857, 1583, 1458, 1419, 1365, 1258, 1135, 1086, 759, 723 cm^{-1}. **^{1}H NMR (δ, $CDCl_3$, 300 MHz)**: 8.62 (d, 1H, J = 4.5 Hz), 8.37 (d, 1H, J = 7.8 Hz), 8.13 (d, 1H, J = 7.8 Hz), 7.67 (t, 1H, J = 8.4 Hz), 7.44 (d, 1H, J = 8.7 Hz), 7.32 (t, 1H, J = 7.5 Hz), 7.21–7.17 (m, 1H), 4.50 (t, 2H, J = 6.9 Hz, —NCH_2), 3.41 (t, 2H, J = 6.6 Hz, —CH_2Br), 1.91–1.84 (m, 4H), 1.52–1.39 (m, 4H). **^{13}C NMR (δ, $CDCl_3$, 100 MHz)**: 152.5, 149.7, 138.9, 134.1, 133.1, 124.6, 124.1, 122.8, 118.8, 117.6, 116.7, 45.7 (—NCH_2), 34.2 (—CH_2Br), 30.1, 28.1, 26.3, 25.8. **Mass spectral data, TOF ES+ *m/z* (%)**: 396 (M^+ + 2).

Elemental analysis: **observed**: C = 51.67%, H = 4.80%, N = 7.05%, S = 8.10%. **Calculated**: C = 51.65%, H = 4.84%, N = 7.09%, S = 8.11%. **Empirical formula**: $C_{17}H_{19}N_2O_2SBr$

5.6 | General Procedure for the Synthesis of 12a–e

Secondary amines (**11a–e**, 3.90 mmol) were added to a well-stirred solution of dimethyl formamide (2 mL) and anhydrous K_2CO_3 (0.538 g, 3.90 mmol) under a nitrogen atmosphere. 10-(6-Bromohexyl)-10*H*-benzo[b]pyrido[2,3-e][1,4]thiazin-5-oxide (**10**) (0.500 g, 1.32 mmol) in 10 mL of dimethyl formamide was added dropwise to the previously stirred solution. The reaction mixture was heated at 40°C under microwave conditions for 1 h (conventional heating at 60°C takes 12 h to complete the reaction). TLC monitored the progress of the reaction. After the reaction, the contents were cooled and quenched with ice water. The crystalline, white-colored solids were separated, and they were filtered and dried to get the desired compounds.

5.6.1 | 10-(6-(Piperidin-1-yl)Hexyl)-10*H*-Benzo[b]Pyrido[2,3-e][1,4]Thiazin-5-Oxide (12a)

Yield 0.429 g (84%), m.p. 68°C–70°C, R_f = 0.40 in chloroform/methanol (90:10). IR ν_{max} (KBr): 2927, 2806, 1575, 1450, 1414, 1219, 1116, 1045, 765, 523, 529 cm^{-1}. ^{1}H NMR (δ, $CDCl_3$, 400 MHz): 8.64–8.62 (dd, 1H, J = 4.8 and 1.5 Hz), 8.22–8.20 (dd, 1H, J = 7.5 and 1.8 Hz), 7.97–7.95 (dd, 1H, 7.5 and 1.5 Hz), 7.70–7.66 (m, 1H), 7.49 (d, 1H, J = 8.7 Hz), 7.31 (t, 1H, J = 7.3 Hz), 7.19–7.16 (m, 1H), 4.68 (m, 2H, —NCH_2), 2.54–2.52 (m, 4H, 2× NCH_2), 2.30 (t, 2H, H_2C—N<), 1.87–1.84 (m, 2H), 1.59–1.57 (m, 4H), 1.56–1.47 (m, 8H). ^{13}C NMR (δ, $CDCl_3$, 100 MHz): 151.9, 147.7, 140.5, 137.7, 133.2, 123.3, 122.3, 117.9, 117.4, 116.4, 59.6, 54.7, 45.6 (—NCH_2), 27.5, 26.9, 26.6, 26.0, 24.5. Mass spectral data, TOF ES+ *m/z* (%): 384 (M^+ + 1). Elemental analysis: observed: C = 68.91%, H = 7.60%, N = 10.95%, S = 8.34%. Calculated: C = 68.89%, H = 7.62%, N = 10.96%, S = 8.36%. Empirical formula: $C_{22}H_{29}N_3OS$.

5.6.2 | 10-(6-Morpholinohexyl)-10*H*-Benzo[b]Pyrido[2,3-e][1,4]Thiazin-5-Oxide (12b)

Yield 0.424 g (83%), m.p. 54°C–56°C, R_f = 0.55 in chloroform/methanol (90:10). IR ν_{max} (KBr): 2925, 2854, 1580, 1450, 1414, 1250, 1116, 1044, 765 cm^{-1}. ^{1}H NMR (δ, $CDCl_3$, 300 MHz): 8.63 (d, 1H, J = 4.5 Hz), 8.21 (d, 1H, J = 7.5 Hz), 7.97 (d, 1H, J = 7.8 Hz), 7.68 (t, 1H, J = 7.8 Hz), 7.48 (d, 1H, J = 8.7 Hz), 7.31 (t, 1H, J = 7.2 Hz), 7.19–7.15 (m, 1H), 4.67–4.65 (m, 2H, —NCH_2), 3.72 (t, 4H, J = 4.2 Hz, 2× OCH_2), 2.44–2.42 (m, 4H, 2× NCH_2), 2.35 (t, 2H, J = 6.5 Hz, H_2C—N<), 1.78–1.69 (m, 4H), 1.55–1.40 (m, 4H). ^{13}C NMR (δ, $CDCl_3$, 75.47 MHz): 151.7, 147.6, 140.1, 137.6, 133.1, 132.1, 123.3, 122.2, 117.9, 117.3, 116.3, 66.8 (2× OCH_2), 59.0, 53.7, 45.3 (—NCH_2), 27.1, 26.7, 26.5, 26.3. Mass spectral data, ESI+ *m/z* (%): 386 (M^+ + 1). Elemental analysis: observed: C = 65.48%, H = 7.02%, N = 10.08%, S = 8.33%. Calculated: C = 65.42%, H = 7.06%, N = 10.90%, S = 8.32%. Empirical formula: $C_{21}H_{27}N_3O_2S$

5.6.3 | 10-(6-Thiomorpholinohexyl)-10*H*-Benzo[b]Pyrido[2,3-e][1,4]Thiazin-5-Oxide (12c)

Yield 0.432 g (81%), m.p. 56°C–58°C, R_f = 0.54 in chloroform/methanol (90:10). IR ν_{max} (film): 2925, 2854, 1580, 1450, 1414, 1250, 1116, 1043, 765 cm^{-1}. ^{1}H NMR (δ, $CDCl_3$, 400 MHz): 8.62–8.61 (dd, 1H, J = 5.0 and 1.8 Hz), 8.20–8.18 (dd, 1H, J = 7.8 and 1.8 Hz), 7.97–7.95 (dd, 1H, J = 7.8 and 1.8 Hz), 7.68–7.64 (m, 1H), 7.47 (d, 1H, J = 8.7 Hz), 7.31 (m, 1H), 7.17–7.14 (m, 1H), 4.64 (m, 2H, —N—CH_2), 2.72–2.67 (m, 8H, thiomorpholine), 2.37 (t, 2H, J = 7.3 Hz, H_2C—N<), 2.01–1.75 (m, 2H), 1.54–1.36 (m, 6H). ^{13}C NMR (δ, $CDCl_3$, 100 MHz): 151.7, 147.6, 140.4, 137.5, 133.1, 132.0, 123.2, 122.2, 117.8, 117.3, 116.2, 59.1, 54.8, 45.2 (N—CH_2), 27.7, 27.1, 26.6, 26.4, 26.1. Mass spectral data, TOF ES+ *m/z* (%): 402 (M^+ + 1). Elemental analysis: observed: C = 62.84%, H = 6.77%, N = 10.44%, S = 15.98%. Calculated: C = 62.81%, H = 6.78%, N = 10.46%, S = 15.97%. Empirical formula: $C_{21}H_{27}N_3OS_2$

5.6.4 | 10-(6-(4-Methylpiperazin-1-yl)Hexyl)-10*H*-Benzo[b]Pyrido[2,3-e][1,4]Thiazin-5-Oxide (12d)

Yield 0.422 g (80%), m.p. 53°C–55°C, R_f = 0.46 in chloroform/methanol (90:10) as the developing solvent. IR ν_{max} (KBr): 2935, 2856, 1578, 1414, 1163, 1045, 1013, 764 cm^{-1}. ^{1}H NMR (δ, DMSO-d_6, 400 MHz): 8.72–8.71 (dd, 1H, J = 5.1 and 2.2 Hz), 8.46–8.44 (dd, 1H, J = 8.0 and 2.2 Hz), 8.05–8.03 (dd, 1H, J = 8.0 and 1.4 Hz), 7.78–7.77 (m, 1H), 7.72 (d, 1H, J = 8.0 Hz), 7.37 (t, 1H, J = 8.0 Hz), 7.34–7.31 (m, 1H), 4.62 (m, 2H, —NCH_2), 2.35–2.31 (m, 8H, 4x NCH_2, piperazine), 2.23 (t, 2H, J = 7.3 Hz, H_2C—N<), 2.15 (s, 3H, N—CH_3), 1.87–1.68 (m, 2H), 1.42–1.32 (m, 6H). ^{13}C NMR (δ, DMSO-d_6, 100 MHz): 151.9, 147.5, 141.4, 137.7, 133.0, 132.2, 123.5, 122.1, 117.7, 117.2, 116.1, 57.6, 56.6, 55.4, 46.0, 45.2 (N—CH_2), 28.3, 27.5, 27.0, 26.8. Mass spectral data, TOF ES+ *m/z* (%): 399 (M^+ + 1). Elemental analysis: observed: C = 66.32%, H = 7.60%, N = 14.02%, S = 8.07%. Calculated: C = 66.30%, H = 7.59%, N = 14.06%, S = 8.05%. Empirical formula: $C_{22}H_{30}N_4OS$.

5.6.5 | 10-(6-(Pyrrolidin-1-yl)Hexyl)-10*H*-Benzo[b]Pyrido[2,3-e][1,4]Thiazin-5-Oxide (12e)

Yield 0.401 g (82%), R_f = 0.36 chloroform/methanol (90:10). IR ν_{max} (KBr): 2927, 1578, 1450, 1415, 1251, 1043, 763, 645 cm^{-1}. ^{1}H NMR (δ, $CDCl_3$, 400 MHz): 8.64–8.63 (dd, 1H, J = 2.2 and 5.1 Hz), 8.22–8.20 (dd, 1H, J = 2.2 and 7.3 Hz), 7.98–7.96 (dd, 1H, J = 1.4 and 8.0 Hz), 7.70–7.66 (m, 1H), 7.49 (d, 1H, J = 8.0 Hz), 7.30 (t, 1H, J = 7.3 Hz), 7.18–7.15 (m, 1H), 4.62–4.56 (m, 2H, N—CH_2), 2.72 (m, 4H, —N(CH_2)$_2$), 2.59 (t, 2H, J = 7.3 Hz), 1.96–1.75 (m, 4H), 1.69–1.64 (m, 2H), 1.51–1.39 (m, 6H). ^{13}C NMR (δ, $CDCl_3$, 100 MHz): 152.0,

147.6, 140.4, 137.5, 133.4, 131.9, 122.4, 117.5, 116.2, 56.0 (—NCH_2), 53.9 (—$N(CH_2)_2$), 27.0, 26.4, 23.3. Observed: C = 59.61%, H = 6.99%, N = 9.55%, S = 5.77%. Calculated: C = 68.26%, H = 7.36%, N = 11.37%, S = 8.68%. **Mass spectral data, LCMS *m/z* (%)**: 370 ($M^+ + 1$). Empirical formula: $C_{21}H_{27}N_3OS$.

5.7 | General Procedure for the Synthesis of 14a–e

Secondary amines (3.78 mmol) were added to a well-stirred solution of dimethyl formamide (2 mL) and anhydrous K_2CO_3 (0.521 g, 3.78 mmol) under a nitrogen atmosphere. 10-(6-Bromohexyl)-10*H*-benzo[b]pyrido[2,3-e][1,4]thiazin-5,5-dioxide (**13**) (0.500 g, 1.27 mmol) in 10 mL of dimethyl formamide was added dropwise to the previously stirred solution. The reaction mixture was heated at 40°C under microwave conditions for 1 h (conventional heating at 60°C takes 12 h to complete the reaction). TLC monitored the progress of the reaction. After the reaction, the contents were cooled and quenched with ice water. The crystalline, white-colored solids were separated, which were filtered and dried to get the desired compounds.

5.7.1 | 10-(6-(Piperidin-1-yl)Hexyl)-10*H*-Benzo[b]Pyrido[2,3-e][1,4]Thiazin-5,5-Dioxide (14a)

Yield 0.465 g (92%), m.p. 78°C–80°C, R_f = 0.61 in chloroform/methanol (90:10). IR ν_{max} (KBr): 2931, 2857, 2811, 1579, 1449, 1419, 1364, 1297, 1116, 1135, 758, 528 cm^{-1}. ^1H NMR (δ, DMSO-d_6, 400 MHz): 8.69–8.68 (dd, 1H, J = 5.12 and 2.2 Hz), 8.37–8.35 (dd, 1H, J = 8.0 and 2.2 Hz), 8.05 (d, 1H, J = 6.5 Hz), 7.75 (t, 1H, J = 6.6 Hz), 7.56 (d, 1H, J = 8.7 Hz), 7.37 (t, 1H, J = 7.3 Hz), 7.31–7.28 (m, 1H), 4.51 (t, 2H, J = 6.9 Hz, —NCH_2), 2.36–2.34 (m, 4H, 2× NCH_2), 2.28 (t, 2H, J = 7.3 Hz, H_2C—N<), 1.88–1.84 (m, 2H), 1.57–1.39 (m, 12H). ^{13}C NMR (δ, $CDCl_3$, 100 MHz): 152.1, 148.9, 138.2, 133.7, 132.3, 123.0, 122.2, 117.9, 117.2, 116.5, 58.8, 54.2, 45.0 (—NCH_2), 26.9, 26.4, 26.2, 25.5, 24.0. Mass spectral data, TOF ES+ *m/z* (%): 400 ($M^+ + 1$). Elemental analysis: observed: C = 66.17%, H = 7.30%, N = 10.51%, S = 8.04%. Calculated: C = 66.13%, H = 7.32%, N = 10.52%, S = 8.03%. Empirical formula: $C_{22}H_{29}N_3O_2S$.

5.7.2 | 10-(6-Morpholinohexyl)-10*H*-Benzo[b]Pyrido[2,3-e][1,4]Thiazin-5,5-Dioxide (14b)

Yield 0.472 g (93%), m.p. 74°C–76°C, R_f = 0.65 in chloroform/methanol (90:10). IR ν_{max} (KBr): 2931, 2857, 2811, 1579, 1449, 1419, 1366, 1297, 1135, 1116, 758, 530 cm^{-1}. ^1H NMR (δ, DMSO-d_6/$CDCl_3$, 300 MHz): 8.64–8.62 (dd, 1H, J = 4.8 and 2.2 Hz), 8.36 (d, 1H, J = 6.8 Hz), 8.11 (d, 1H, J = 6.6 Hz), 7.70–7.69 (m, 1H), 7.48–7.34 (m, 2H), 7.22–7.20 (m, 1H), 4.50 (m, 2H, —NCH_2), 3.72 (m, 4H, 2× OCH_2), 2.42–2.40 (m, 4H, 2× NCH_2), 2.32 (t, 2H, H_2C—N<), 1.88–1.86 (m, 2H), 1.50–1.47 (m, 6H). ^{13}C NMR (δ, DMSO-d_6/$CDCl_3$, 75.47 MHz): 151.7, 148.8, 138.1, 133.3, 132.2, 123.7, 123.2, 122.0, 117.9, 116.8, 116.0, 66.5 (2× OCH_2), 58.5, 53.4, 45.1 (–NCH_2), 26.7, 26.4, 26.2, 26.0. Mass spectral data, ESI+ *m/z* (%): 402 ($M^+ + 1$). Elemental analysis: observed: C = 62.84%, H = 6.77%, N = 10.45%, S = 7.98%. Calculated: C = 62.82%, H = 6.78%, N = 10.47%, S = 7.99%. Empirical formula: $C_{21}H_{27}N_3O_3S$.

5.7.3 | 10-(6-Thiomorpholinohexyl)-10*H*-Benzo[b]Pyrido[2,3-e][1,4]Thiazin-5,5-Dioxide (14c)

Yield 0.484 g (91%), m.p. 54°C–56°C, R_f = 0.56 in chloroform/methanol (95:5). IR ν_{max} (KBr): 2925, 2854, 1583, 1458, 1419, 1370, 1297, 1165, 1137, 759, 723 cm^{-1}. ^1H NMR (δ, DMSO-d_6, 300 MHz): 8.73 (dd, 1H), 8.42 (d, 1H, J = 6.6 Hz), 8.03 (d, 1H, J = 6.9 Hz), 7.78–7.72 (m, 2H), 7.39–7.37 (m, 2H), 4.52 (m, 2H, —NCH_2), 2.73–2.54 (m, 8H, thiomorpholine), 2.28 (m, 2H, H_2C—N<), 1.71–1.69 (m, 2H), 1.61–1.47 (m, 6H). ^{13}C NMR (δ, DMSO-d_6, 75.47 MHz): 154.3, 148.5, 137.8, 134.1, 132.7, 123.6, 122.8, 122.6, 117.8, 117.7, 117.2, 58.3, 54.5, 44.3 (—NCH_2), 27.1, 26.4, 25.7, 25.0. Mass spectral data, TOF ES+ *m/z* (%): 418 ($M^+ + 1$). Elemental analysis: observed: C = 60.40%, H = 6.52%, N = 10.06%, S = 15.36%. Calculated: C = 60.42%, H = 6.50%, N = 10.08%, S = 15.38%. Empirical formula: $C_{21}H_{27}N_3O_2S_2$.

5.7.4 | 10-(6-(4-Methylpiperazin-1-yl)Hexyl)-10*H*-Benzo[b]Pyrido[2,3-e][1,4]Thiazin-5,5-Dioxide (14d)

Yield 0.484 g (92%), m.p. 52 C–54 C, R_f = 0.50 chloroform/methanol (90:10). IR ν_{max} (KBr): 2932, 2853, 2794, 1582, 1458, 1419, 1297, 1164, 1135, 1086, 759 cm^{-1}. ^1H NMR (δ, DMSO-d_6, 300 MHz): 8.75 (d, 1H, J = 3.0 Hz), 8.44 (d, 1H, J = 7.2 Hz), 8.05 (d, 1H, J = 7.5 Hz), 7.84–7.72 (m, 2H), 7.45–7.31 (m, 2H), 4.55 (m, 2H, —NCH_2), 2.26–2.15 (m, 8H, 2× $(NCH_2)_2$, piperazine), 2.11 (N–CH_3), 1.75 (m, 2H, H_2C—N<), 1.75 (m, 2H), 1.37–1.21 (m, 6H). ^{13}C NMR (δ, DMSO-d_6, 75.47 MHz): 152.7, 148.6, 137.9, 134.2, 132.7, 123.6, 122.8, 122.7, 117.8, 117.7, 117.3, 57.7, 54.7, 52.7, 45.9, 45.7 (—NCH_2), 26.5, 26.3, 26.2, 25.8. Mass spectral data, TOF ES+ *m/z* (%): 415 ($M^+ + 1$). Elemental analysis: observed: C = 63.78%, H = 7.23%, N = 13.0%, S = 7.71%. Calculated: C = 63.74%, H = 7.29%, N = 13.51%, S = 7.73%. Empirical formula: $C_{22}H_{30}N_4O_2S$.

5.7.5 | 10-(6-(Pyrrolidin-1-yl)Hexyl)-10*H*-Benzo[b]Pyrido[2,3-e][1,4]Thiazine-5,5-Dioxide (14e)

Yield 0.465 g (92%), R_f = 0.54 chloroform/methanol (90:10) as a developing solvent. IR ν_{max} (KBr): 2929, 2857, 2780, 1582, 1458, 1419, 1297, 1165, 1029, 758 cm^{-1}. ^1H NMR (δ, DMSO-d_6, 300 MHz): 8.63–8.62 (dd, 1H, J = 1.8 and 4.7 Hz), 8.39–8.37 (dd, 1H, J = 1.8 and 7.8 Hz), 8.15–8.13 (dd, 1H, J = 1.4 and 7.9 Hz), 7.69–7.65 (m, 1H), 7.45 (d, 1H, J = 7.4 Hz), 7.34–7.30 (m, 1H), 7.21–7.17 (m, 1H), 4.49 (t, 2H, N—CH_2), 2.51 (m, 4H), 2.26 (t, 2H, N—CH_2, J = 7.6 Hz), 1.90–1.87 (m, 2H), 1.80–1.77 (m, 4H), 1.65–1.61 (m, 6H). ^{13}C NMR (δ, DMSO-d_6, 75.47 MHz): 152.2, 149.4, 138.5, 133.7, 132.7, 124.2, 123.8, 122.5, 118.4, 117.2, 56.4, 54.1, 45.5 (—$N(CH_2)_2$), 28.5, 27.2, 26.8, 26.6, 23.4. Mass spectral data, TOF ES+ *m/z* (%): 386 ($M^+ + 1$, 100). Elemental analysis: observed: C = 56.09%, H = 6.10%, N = 9.06%, S = 7.12%. Calculated: C = 65.42%, H = 7.06%, N = 10.90%, S = 8.32%. Empirical formula: $C_{21}H_{27}N_3O_2S$.

5.8 | Molecular Docking Study

The binding affinity and interaction profiles of synthesized compounds (12a–e and 14a–e) with the *E. coli* DNA gyrase enzyme (PDB ID: 7P2M) were investigated through molecular docking

studies using AutoDock 4.2 [64]. The crystal structure of *E. coli* DNA gyrase was obtained from the Protein Data Bank and inspected for missing residues using ChimeraX 1.8 [65]. Missing residues at positions 1–7 (MET1, SER2, ASN3, SER4, TYR5, ASP6, SER7), 99–116 (HIS99, ALA100, GLY101, GLY102, LYS103, PHE104, ASP105, ASP106, ASN107, SER108, TYR109, LYS110, VAL111, SER112, GLY113, GLY114, LEU115, HIS116), and 219–220 (GLU219, GLY220) were modeled using Modeler 10.6 to restore the complete structure [66]. Unnecessary components, such as water molecules and co-crystallized ligands, were removed.

Energy minimization of the protein was performed in UCSF Chimera 1.17.1 using the steepest descent and conjugate gradient algorithms for 5000 steps [67, 68]. Hydrogen atoms were added, and Gasteiger charges were assigned to ensure compatibility with AutoDock. The final energy-minimized protein structure was saved in PDB format for docking studies.

The 2D chemical structures of the synthesized compounds were drawn in ChemDraw 22.0.0 and converted into 3D geometries using Chem3D. Energy minimization of the ligands was carried out using the MMFF94 force field to optimize their conformations. The minimized ligands were then saved in PDBQT format for docking studies.

The active site of *E. coli* DNA gyrase was defined on the basis of prior mapping. A grid box was generated with dimensions of $50 \times 70 \times 52$ Å and center coordinates X: −18.6026, Y: −15.0457, Z: 6.5532, using a grid spacing of 0.375 Å. The synthesized compounds were docked into the active site of the enzyme, and the lowest energy docking conformations were recorded. Docking results were analyzed to evaluate binding energies and interaction patterns between the ligands and the enzyme's active site. Key interactions, such as hydrogen bonds, hydrophobic interactions, and van der Waals forces, were examined to assess binding efficiency.

5.9 | MD Simulation Studies

MD simulations were performed on the protein–ligand complexes using GROMACS 2020 software, employing the CHARMM-36 M force field for atomic interaction modeling [69]. The initial docking conformations, selected based on the most negative binding energy (indicating maximum binding affinity), served as starting structures for the simulations. Topology files for the ligands, including compound 12c and ciprofloxacin, were generated using the CHARMM-GUI web server to ensure accurate representation of the ligand parameters and their interactions within the protein environment [70].

The simulation systems were solvated using the TIP3P water model, and periodic boundary conditions were applied in all directions to simulate a realistic biological environment. The systems were neutralized by adding appropriate numbers of sodium (Na^+) and chloride (Cl^-) ions using the Monte Carlo ion placement method. Energy minimization of the solvated systems was conducted using the steepest descent algorithm for 5,00,000 steps to eliminate steric clashes and stabilize the initial configuration. The LINCS algorithm was applied during energy minimization to constrain hydrogen bond lengths and preserve the structural integrity of the protein–ligand complexes [71].

Equilibration of the systems was performed in two sequential phases: the canonical ensemble (NVT) and the isothermal-isobaric ensemble (NPT). Each phase was executed for 1 ns, with the temperature maintained at 310.15 K using a velocity-rescaling thermostat and the pressure set at 1 bar using the Berendsen barostat. A leap-frog integrator was used for numerical stability during these steps. Following equilibration, a 200-ns production MD simulation was conducted under constant temperature and pressure conditions to capture the long-term behavior of the complexes.

Trajectory analyses were performed to evaluate the structural stability and flexibility of the complexes. RMSD and RMSF were calculated to monitor protein–ligand stability and residue-level flexibility using the gmx_rms and gmx_rmsf modules, respectively. Intermolecular hydrogen bonds were quantified using gmx_hbond, whereas SASA and Rg were computed using gmx_sasa and gmx_gyrate to analyze the surface exposure and compactness of the complexes. All MD analysis plots were generated using the QtGrace tool to ensure clear graphical representation of results [72, 73].

Acknowledgments

We thank the Department of Chemistry and Biochemistry at Augusta University and the Department of Chemistry at Delhi University for their support. The work was also supported by the Augusta University Provost's office and the Translational Research Program of the Department of Medicine, Medical College of Georgia at Augusta University.

Conflicts of Interest

The authors declare no conflicts of interest.

Data Availability Statement

Data will be made available on request.

References

1. A. M. Socha, N. Y. Tan, K. L. LaPlante, and J. K. Sello, "Diversity-Oriented Synthesis of Cyclic Acyldepsipeptides Leads to the Discovery of a Potent Antibacterial Agent," *Bioorganic & Medicinal Chemistry* 18 (2010): 7193–7202.

2. D. A. Goldmann and W. C. Huskins, "Control of Nosocomial Antimicrobial-Resistant Bacteria: A Strategic Priority for Hospitals Worldwide," *Clinical Infectious Diseases* 24 (1997): S139–S145.

3. K. W. K. Tang, B. C. Millar, and J. E. Moore, "Antimicrobial Resistance (AMR)," *British Journal of Biomedical Science* 80 (2023): 11387.

4. N. A. R. Gow, C. Johnson, J. Berman, et al., "The Importance of Antimicrobial Resistance in Medical Mycology," *Nature Communications* 13 (2022): 5352.

5. M. C. Fisher, A. Alastruey-Izquierdo, J. Berman, et al., "Tackling the Emerging Threat of Antifungal Resistance to Human Health," *Nature Reviews Microbiology* 20 (2022): 557–571.

6. J. Xuan, W. Feng, J. Wang, et al., "Antimicrobial Peptides for Combating Drug-Resistant Bacterial Infections," *Drug Resistance Updates* 68 (2023): 100954.

7. A. Gaurav, P. Bakht, M. Saini, S. Pandey, and R. Pathania, "Role of Bacterial Efflux Pumps in Antibiotic Resistance, Virulence, and Strategies to Discover Novel Efflux Pump Inhibitors," *Microbiology (Reading, England)* 169 (2023): 001333.

8. Z. Pang, R. Raudonis, B. R. Glick, T. J. Lin, and Z. Cheng, "Antibiotic Resistance in *Pseudomonas aeruginosa*: Mechanisms and Alternative Therapeutic Strategies," *Biotechnology Advances* 37 (2019): 177–192.

9. G. Muteeb, M. T. Rehman, M. Shahwan, and M. Aatif, "Origin of Antibiotics and Antibiotic Resistance, and Their Impacts on Drug Development: A Narrative Review," *Pharmaceuticals* 16 (2023): 1615.

10. M. A. Salam, M. Y. Al-Amin, M. T. Salam, et al., "Antimicrobial Resistance: A Growing Serious Threat for Global Public Health," *Healthcare (Basel, Switzerland)* 11 (2023): 1946.

11. D. C. Nwobodo, M. C. Ugwu, C. O. Anie, et al., "Antibiotic Resistance: The Challenges and Some Emerging Strategies for Tackling a Global Menace," *Journal of Clinical Laboratory Analysis* 36 (2022): e24655.

12. J. Jampilek, "Heterocycles in Medicinal Chemistry," *Molecules (Basel, Switzerland)* 24 (2019): 3839.

13. A. Rusu, I. M. Moga, L. Uncu, and G. Hancu, "The Role of Five-Membered Heterocycles in the Molecular Structure of Antibacterial Drugs Used in Therapy," *Pharmaceutics* 15 (2023): 2554.

14. E. Kabir and M. Uzzaman, "A Review on Biological and Medicinal Impact of Heterocyclic Compounds," *Results in Chemistry* 4 (2022): 100606.

15. M. M. Li, X. Chen, Y. Deng, and J. Lu, "Recent Advances of N-Heterocyclic Carbenes in the Applications of Constructing Carbo- and Heterocyclic Frameworks With Potential Biological Activity," *RSC Advances* 11 (2021): 38060–38078.

16. L. Aguilar-Vega, L. E. López-Jácome, B. Franco, et al., "Antibacterial Properties of Phenothiazine Derivatives Against Multidrug-Resistant *Acinetobacter baumannii* Strains," *Journal of Applied Microbiology* 131 (2021): 2235–2243.

17. K. Venkatesan, VSV Satyanarayana, A. Sivakumar, C. Ramamurthy, and C. Thirunavukkarusu, "Synthesis, Spectral Characterization and Antitumor Activity of Phenothiazine Derivatives," *Journal of Heterocyclic Chemistry* 57 (2020): 2722.

18. A. N. Edinoff, G. Armistead, C. A. Rosa, et al., "Phenothiazines and Their Evolving Roles in Clinical Practice: A Narrative Review," *Health Psychology Research* 10 (2022): 38930.

19. W. M. B. Reid, J. B. Wright, H. G. Kolloff, and J. H. Hunter, "Histamine Antagonists. II. N-(Pyrrolidylalkyl)-phenothiazines," *Journal of the American Chemical Society* 70 (1948): 3100–3102.

20. L. Zeltzer, S. LeBaron, and P. M. Zeltzer, "Paradoxical Effects of Prophylactic Phenothiazine Antiemetics in Children Receiving Chemotherapy," *Journal of Clinical Oncology: Official Journal of the American Society of Clinical Oncology* 2 (1984): 930–936.

21. H. O. J. Collier, "Depression of Neuro-Muscular Transmission in a Crab by Phenothiazine," *Nature* 146 (1940): 232–233.

22. D. G. Friend, "Polypharmacy—Multiple-Ingredient and Shotgun Prescriptions," *New England Journal of Medicine* 260 (1959): 1015–1018.

23. A. Zięba, Z. Czuba, and W. Król, "In Vitro Antimicrobial Activity of Novel Azaphenothiazine Derivatives," *Acta Poloniae Pharmaceutica–Drug Research* 69 (2012): 1149–1152.

24. M. Jeleń, K. Pluta, M. Zimecki, B. Morak-Młodawska, J. Artym, and M. Kocięba, "6-Substituted 9-Fluoroquino[3,2-b]Benzo[1,4]Thiazines Display Strong Antiproliferative and Antitumor Properties," *European Journal of Medicinal Chemistry* 89 (2015): 411–420.

25. M. Otręba, L. Kośmider, and A. Rzepecka-Stojko, "Antiviral Activity of Chlorpromazine, Fluphenazine, Perphenazine, Prochlorperazine, and Thioridazine Towards RNA-Viruses. A Review," *European Journal of Pharmacology* 887 (2020): 173553.

26. A. J. Warman, T. S. Rito, N. E. Fisher, et al., "Antitubercular Pharmacodynamics of Phenothiazines," *Journal of Antimicrobial Chemotherapy* 68 (2013): 869–880.

27. K. Venkatesan, V. S. V. Satyanarayana, and A. Sivakumar, "Synthesis and Biological Evaluation of Novel Phenothiazine Derivatives as Potential Antitumor Agents," *Polycyclic Aromatic Compounds* 43 (2023): 850–859.

28. K. Venkatesan, K. M. Kumar, and A. Sivakumar, "Synthesis, Characterization and Anticancer Molecular Docking Studies of Phenothiazine Derivatives–A Green Chemical Approach," *Chemistry Select* 8 (2023): e202302613.

29. K. Pluta, M. Jeleń, B. Morak-Młodawska, et al., "Azaphenothiazines—Promising Phenothiazine Derivatives. An Insight Into Nomenclature, Synthesis, Structure Elucidation and Biological Properties," *European Journal of Medicinal Chemistry* 138 (2017): 774–806. (Review and the references cited within).

30. K. Kushwaha, R. Sakhuja, and S. C. Jain, "Synthesis and Antimicrobial Activity of Novel *bis*-Azaphenothiazines," *Medicinal Chemistry Research* 22 (2013): 4459–4467.

31. B. Morak-Młodawska, K. Pluta, M. Latocha, M. Jeleń, "Synthesis, Spectroscopic Characterization, and Anticancer Activity of New 10-Substituted 1,6-Diazaphenothiazines," *Medicinal Chemistry Research* 25 (2016): 2425–2433.

32. B. Morak-Młodawska, K. Pluta, M. Latocha, K. Suwińska, M. Jeleń, and D. Kuśmierz, "3,6-Diazaphenothiazines as Potential Lead Molecules—Synthesis, Characterization and Anticancer Activity," *Journal of Enzyme Inhibition and Medicinal Chemistry* 31 (2016): 1512–1519.

33. M. Jeleń, K. Pluta, M. Zimecki, B. Morak-Młodawska, J. Artym, and M. Kocięba, "Synthesis and Selected Immunological Properties of Substituted Quino[3,2-b]Benzo[1,4]Thiazines," *European Journal of Medicinal Chemistry* 63 (2013): 444–456.

34. J. McKenzie, N. Feeder, and C. A. Hunter, "H-Bond Competition Experiments in Solution and the Solid State," *CrystEngComm* 18 (2016): 394–397.

35. C. Laurance, K. A. Brameld, J. Granton, J. L. Questel, and E. Renault, "The p KBHX Database: Toward a Better Understanding of Hydrogen-Bond Basicity for Medicinal Chemists," *Journal of Medicinal Chemistry* 52 (2009): 4073–4086.

36. F. Vittorio, M. S. Pappalardo, G. Ronsisvalle, A. Caruso, M. G. Leone, and M. Amico-Roxas, "Chemical and Pharmacological Investigations on 2H-Pyridazino[4,5- b][1,4]Benzothiazin-1-(10H)-one Derivatives," *Farmaco* 44 (1989): 911–932.

37. Y. C. Tong and W. C. Calif, Oxides of Primary 10*H*-Pyrazino[2,3-b][1,4]Benzothiazine. US Patent (United States Patent and Trademark Office, 1974).

38. H. Agrawal, A. K. Yador, and L. Prakash, "An Elegant Synthesis of Some New Potential Biologically Active Pyrido[3,2-b][1,4]Benzothiazine Derivatives and Their Nucleosides by Phase Transfer Catalysis," *Heterocyclic Communication* 4 (1998): 589–594.

39. R. J. Chorvat, B. N. Desai, S. E. Radak, J. Bloss, J. Hirsch, and S. Tenen, "Synthesis, Benzodiazepine Receptor Binding, and Anticonvulsant Activity of 2,3-Dihydro-3-oxo-5*H*-Pyrido[3,4-b][1,4]Benzothiazine-4-Carbonitriles," *Journal of Medicinal Chemistry* 26 (1983): 845–850.

40. A. Gupta, R. Sakhuja, and S. C. Jain, "Microwave-Assisted Synthesis of 10-(Phthalimidoalkyl)-Halosubstitutedpyrido [3,2-b][1,4]-Benzothiazine in Dry Media," *Synthetic Communications* 37 (2007): 4059–4069.

41. K. Kushwaha, N. K. Kaushik, N. Kaushik, et al., "Novel Aminoalkylated Azaphenothiazines as Potential Inhibitors of T98G, H460 and SNU80 Cancer Cell Lines In Vitro," *Bioorganic & Medicinal Chemistry Letters* 26 (2016): 2237–2244.

42. CLSI. *Methods for Dilution Antimicrobial Susceptibility Tests for Bacteria Grow Aerobically*. 11th ed. CLSI standard M07 (Chemical and Laboratory Standards Institute, 2018).

43. M. A. Ibrahim, S. S. Panda, A. S. Birs, et al., "Synthesis and Antibacterial Evaluation of Amino Acid–Antibiotic Conjugates," *Bioorganic & Medicinal Chemistry Letters* 24 (2014): 1856–1861.

44. M. A. Ibrahim, S. S. Panda, A. A. Oliferenko, et al., "Macrocyclic Peptidomimetics With Antimicrobial Activity: Synthesis, Bioassay, and Molecular Modeling Studies," *Organic & Biomolecular Chemistry* 13 (2015): 9492–9503.

45. P. K. Parida, D. Paul, and D. Chakravorty, "The Natural Way Forward: Molecular Dynamics Simulation Analysis of Phytochemicals From Indian Medicinal Plants as Potential Inhibitors of SARS-CoV -2 Targets," *Phytotherapy Research* 34 (2020): 3420–3433.

46. J. Cummings, J. P. S. Aisen, B. DuBois, et al., "Drug Development in Alzheimer's Disease: The Path to 2025," *Alzheimer's Research & Therapy* 8 (2016): 1–12.

47. A. L. Flint, D. W. Hansen, L. D. Brown, L. E. Stewart, E. Ortiz, and S. S. Panda, "Modified Curcumins as Potential Drug Candidates for Breast Cancer: An Overview," *Molecules* 27 (2022): 8891.

48. A. Daina, O. Michielin and V. Zoete, "SwissADME: A Free Web Tool to Evaluate Pharmacokinetics, Drug-Likeness and Medicinal Chemistry Friendliness of Small Molecules," *Scientific Reports* 7 (2017): 42717.

49. S. S. Panda, E. Thomas, and A. M. Pham, "Microwave-Assisted Synthesis of Tri-Substituted 1,3,5-Triazines From Metformin Using Benzotriazole Chemistry," *Reactions* 3 (2022): 516–524.

50. G. M. Maggiora, "Introduction to Molecular Similarities and Chemical Space," in *Foodinformatics: Applications of Chemical Information to Food Chemistry*, eds. K. Martinez-Mayorga and J. L. Medina-Franco (Springer International Publishing, 2014), 1–81.

51. A. M. Virshup, J. Contreras-García, P. Wipf, W. Yang, and D. N. Beratan, "Stochastic Voyages Into Uncharted Chemical Space Produce a Representative Library of All Possible Drug-Like Compounds," *Journal of the American Chemical Society* 135 (2013): 7296–7303.

52. J. L. Medina-Franco, A. L. Chávez-Hernández, E. López-López, and F. I. Saldívar-González, "Chemical Multiverse: An Expanded View of Chemical Space," *Molecular Informatics* 41 (2022): e2200116.

53. P. D. Tamma, E. Avdic, D. X. Li, K. Dzintars, and S. E. Cosgrove, "Association of Adverse Events With Antibiotic Use in Hospitalized Patients," *JAMA Internal Medicine* 177 (2017): 1308–1315.

54. K. Cooper and W. M. Bennett, "Nephrotoxicity of Common Drugs Used in Clinical Practice," *Archives of Internal Medicine* 147 (1987): 1213–1218.

55. S. David, J. P. Hamilton, "Drug-Induced Liver Injury," *US Gastroenterology and Hepatology Review* 6 (2010): 73–80.

56. K. J. Downes, M. Hayes, J. C. Fitzgerald, et al., "Mechanisms of Antimicrobial-Induced Nephrotoxicity in Children," *Journal of Antimicrobial Chemotherapy* 75 (2020): 1–13.

57. European Association for the Study of the Liver, "Electronic Address: easloffice@easloffice.eu; Clinical Practice Guideline Panel: Chair: Panel members; EASL Governing Board Representative: EASL Clinical Practice Guidelines: Drug-Induced Liver Injury," *Journal of Hepatology* 70, no. 6: (2019): 1222–1261.

58. R. L. Mehta, L. Awdishu, A. Davenport, et al., "Phenotype Standardization for Drug-Induced Kidney Disease," *Kidney International* 88 (2015): 226–234.

59. M. F. Grill and R. K. Maganti, "Neurotoxic Effects Associated With Antibiotic Use: Management Considerations," *British Journal of Clinical Pharmacology* 72 (2011): 381–393.

60. P. Banerjee, E. Kemmler, M. Dunkel, and R. Preissner, "ProTox 3.0: A Webserver for the Prediction of Toxicity of Chemicals," *Nucleic Acids Research* 52 (2024): W513–W520.

61. A. Gupta, R. Sakhuja, K. Kushwaha, and S. C. Jain, "Microwave-Assisted Synthesis of Azoniaspiro Compounds Using a Novel Catalyst, 1-Azaphenothiazine," *Synthetic Communications* 41 (2011): 411–416.

62. S. C. Jain, R. Kumar, R. Goswami, et al., "Synthesis of Novel Non-Isoprenoid Phenolic Acids and 3-Alkylpyridines," *Pure and Applied Chemistry* 77 (2005): 185–193.

63. W. Mohr, C. R. Horn, J. Stahl, and J. A. Gladysz, "Convenient and Convergent Syntheses of Long-Chain α, ω-Dibromides and Diphosphines of the Formula X (CH2) nX (n = 18–32)," *Synthesis* 8 (2003): 1279–1285.

64. A. E. Cotman, M. Durcik, D. Benedetto Tiz, et al., "Discovery and Hit-to-Lead Optimization of Benzothiazole Scaffold-Based DNA Gyrase Inhibitors With Potent Activity Against *Acinetobacter baumannii* and *Pseudomonas aeruginosa*," *Journal of Medicinal Chemistry* 66 (2023): 1380–1425.

65. E. F. Pettersen, T. D. Goddard, C. C. Huang, et al., "UCSF ChimeraX: Structure Visualization for Researchers, Educators, and Developers," *Protein Science* 30 (2021): 70–82.

66. N. Eswar, B. Webb, M. A. Marti-Renom, et al., *Current Protocols in Bioinformatics* (Wiley, 2016).

67. D. H. J. Mackay, A. J. Cross, and A. T. Hagler, "The Role of Energy Minimization in Simulation Strategies of Biomolecular Systems," in *Prediction of Protein Structure and the Principles of Protein Conformation*, ed. G. D. Fasman (Springer, 1989), 317–358.

68. E. F. Pettersen, T. D. Goddard, C. C. Huang, et al., "UCSF Chimera—A Visualization System for Exploratory Research and Analysis," *Journal of Computational Chemistry* 25 (2004): 1605–1612.

69. M. J. Abraham, T. Murtola, R. Schulz, et al., "GROMACS: High Performance Molecular Simulations Through Multi-Level Parallelism From Laptops to Supercomputers," *SoftwareX* 1–2 (2015): 19–25.

70. S. Jo, T. Kim, V. G. Iyer, and W. Im, "CHARMM-GUI: A Web-Based Graphical User Interface for CHARMM," *Journal of Computational Chemistry* 29 (2008): 1859–1865.

71. B. Hess, H. Bekker, H. J. Berendsen, and J. G. Fraaije, "LINCS: A Linear Constraint Solver for Molecular Simulations," *Journal of Computational Chemistry* 18 (1997): 1463–1472.

72. P. Turner, XMGRACE, Version 5.1.19. Center for Coastal and Land-Margin Research, Oregon Graduate Institute of Science and Technology, Beaverton, OR. 2 (2005): 19.

73. B. Das, A. T. Mathew, A. T. Baidya, B. Devi, R. R. Salmon, and R. Kumar, "Artificial Intelligence Assisted Identification of Potential tau Aggregation Inhibitors: Ligand-and Structure-Based Virtual Screening, In Silico ADME, and Molecular Dynamics Study," *Molecular Diversity* 28 (2024): 2013–2031.

Supporting Information

Additional supporting information can be found online in the Supporting Information section.